Cerebral Cortex Advance Access published June 18, 2007

Cerebral Cortex
doi:10.1093/cercor/bhm081

Functional Organization of Color Domains in V1 and V2 of Macaque Monkey Revealed by Optical Imaging

Haidong D. Lu and Anna W. Roe

Department of Psychology, Vanderbilt University, Nashville, TN, USA

Areas V1 and V2 of Macaque monkey visual cortex are characterized by unique cytochrome-oxidase (CO)–staining patterns. Initial electrophysiological studies associated CO blobs in V1 with processing of surface properties such as color and brightness and the interblobs with contour information processing. However, many subsequent studies showed controversial results, some supporting this proposal and others failing to find significant functional differences between blobs and interblobs. In this study, we have used optical imaging to map color-selective responses in V1 and V2. In V1, we find striking "blob-like" patterns of color response. Fine alignment of optical maps and CO-stained tissue revealed that color domains in V1 strongly associate with CO blobs. We also find color domains in V1 align along centers of ocular dominance columns. Furthermore, color blobs in V1 have low orientation selectivity and do not overlap with centers of orientation domains. In V2, color domains coincide with thin stripes; orientation-selective domains coincide with thick and pale stripes. We conclude that color and orientation-selective responses are preferentially located in distinct CO compartments in V1 and V2. We propose that the term "blob" encompasses both the concept of "CO blob" and "color domain" in V1.

Keywords: blobs, color, cytochrome-oxidase, optical imaging, thin stripes

Introduction

Following the discovery of cytochrome-oxidase (CO) blobs (Wong-Riley 1979, referred to as "puffs" by Wong-Riley and as "patches" by Horton and Hubel 1981) in Macaque monkey visual cortex, Livingstone and Hubel (1984) reported in their electrophysiological studies of V1 that blobs were characterized by a predominance of color-selective neurons which lacked strong orientation selectivity, whereas interblobs were characterized by a preponderance of orientation-selective cells that were not color selective. They further reported (Hubel and Livingstone 1987) functional distinctions within V2, whereby thin stripes were color selective and poor in orientation selectivity and pale and thick stripes were orientation selective and less selective for color. This proposed dichotomy led to a number of studies, some of which supported and others which contradicted these findings. This controversy has continued without apparent resolution (e.g., see Sincich and Horton 2005).

At least 2 issues require resolution. The first issue centers on whether there is functional segregation of color and orientation within V1 and within V2. A second issue is the degree of correlation, if any, of color and orientation preference with CO blobs and interblobs, respectively. Findings from some studies support functional segregation. Blobs were reported to contain many color-selective cells that prefer low spatial frequencies and exhibit high contrast sensitivity (Livingstone and Hubel 1984; Tootell, Silverman, et al. 1988; Silverman et al. 1989; Born and Tootell 1991; Edwards et al. 1995; cf. Shoham et al. 1997). Consistent with these studies, 2-deoxyglucose (Tootell, Hamilton, et al. 1988; Tootell, Switkes, et al. 1988; Tootell and Hamilton 1989) and optical imaging methods (Malach et al. 1994; Roe and Ts'o 1995, 1999; Roe 2003; Ts'o et al. 2001; Xiao et al. 2003; Xu et al. 2004; Lu and Roe 2007 for review) found that blobs in V1 are preferentially activated by color stimuli and low spatial frequency stimuli.

Other studies, however, failed to find a clear functional segregation of color- and orientation-selective cells (Levitt et al. 1994; Leventhal et al. 1995; Gegenfurtner et al. 1996; Friedman et al. 2003). These studies reported no significant difference in the distribution of functional properties between blobs and interblobs and between the different cytochrome stripes. Many of the studies failing to see functional segregation were single unit electrophysiological studies. The different conclusions reached by various single unit studies can arise from sampling issues, differences in methodology for localization of recording sites with respect to CO patterns, and differences in receptive field characterization methodology.

Regarding the issue of correspondence with blobs, previous studies of color activation in V1 had provided evidence that color-activated domains align with CO domains (Tootell, Silverman, et al. 1988). However, other studies had found poorer correspondence (Landisman and Ts'o 2002a, 2002b). Landisman and Ts'o reported a high degree of overlap of the color patches with the CO blobs. They found that color patches were often larger than CO blobs, sometimes spanning 2 neighboring blobs and even crossed ocular dominance columns to encompass 2 blobs of different eye preference. Furthermore, they found no direct relationship between the layout of orientation and color selectivity and poor correlation of color and orientation with ocular dominance maps. Furthermore, most of the maps encompassed relatively small fields of view, limiting the ability to infer global correspondence of color blobs and CO blobs. Although larger fields of view have been provided in 2-DG studies (Tootell, Silverman, et al. 1988), no detailed alignment of the 2-DG image and CO blob pattern was performed. A large field of view of aligned optical maps and CO tissue would speak to this issue more fully.

In this study, we have addressed the issue by using intrinsic signal optical imaging of color and orientation response in V1 and V2 of the Macaque monkey followed by detailed alignment of optical maps with CO-stained tissue. We find good alignment of color blobs with CO blobs in V1 and color domains with thin stripes in V2. We also find that color domains align with regions of

low orientation selectivity in both V1 and V2. These findings suggest significant functional segregation of blobs and interblobs in V1 and the thin and thick/pale stripes in V2. Some of these results have been previously reported in abstract form (Roe and Lu 2006).

Methods

Animal Preparation

Five Macaque monkeys (4 *Macaca fascicularis*, 1 *Macaca mulatta* [case 5]) were anesthetized (thiopental sodium, 1–2 mg/kg/h iv and isoflurane, 0–1%), paralyzed with vercuronium bromide (0.05 mg/kg/h iv), and artificially ventilated. Anesthetic depth was assessed continuously via implanted wire electroencephalography electrodes, end-tidal CO_2, oximetry and heart rate monitoring, and by regular testing for response to toe pinch. Eyes were dilated (atropine sulfate) and fitted with contact lenses of appropriate curvature (Danker Laboratories Inc, Sarasota, FL) to focus on a computer screen. Eyes were aligned by converging the receptive fields (RFs) of a binocular V1 neuron with a Risley prism over one eye. Alignment was checked before and after each recording. Craniotomy and durotomy were performed to expose visual areas V1 and V2 (near the lunate sulcus). In one case a chronic chamber was implanted. All surgical and experimental procedures conformed to the guidelines of the National Institute of Health (NIH) and were approved by the Vanderbilt Animal Care and Use Committees.

Visual Stimuli

Full screen drifting sinewave gratings were created using custom-made computer programs (STIM, Kaare Christian or in Matlab, Dan Shima) and presented on a CRT monitor (Barco Calibrator PCD-321, Belgium). The stimulus screen was Gamma corrected using (Minolta Chroma Meter CS-100, Ramsey, NJ) photometer and positioned 38 inches from the eyes. Screen extent spanned 24 × 18° visual field. In each experiment, electromechanical shutters were placed in front of the eyes for monocular stimulation to reveal ocular dominance maps.

Two sets of gratings were used. The first set comprised high contrast monochromatic sinusoidal (Black-White) gratings that were used to reveal ocular dominance and orientation map (except for case 3, in which a 1.25 c/deg thin white line grating drifted at 0.8 Hz was used). These gratings were 1.5 c/deg drifted at 2 Hz. Four orientations (0, 45, 90, and 135) were presented in a randomly interleaved order. During interstimulus interval and during the blank condition, eye-shutters were closed. Each shutter (either left eye or right eye) was opened for stimulus presentation to each eye (Roe and Ts'o 1995; Landisman and Ts'o 2002a). Peak and minimum luminance of the black–white grating were 60 and 0 cd/m^2. Mean luminance for all stimuli, including the blank stimulus (uniform gray screen), was 30 cd/m^2.

The second set of stimuli comprised both red–green and black–white gratings for revealing color domains. These gratings had the same low spatial frequency (0.15 c/deg for cases 1, 2, and 3 and 0.5 c/deg for cases 4 and 5), drifting temporal frequency (0.5 Hz for cases 1, 2, and 3 and 1 Hz for cases 4 and 5), and mean luminance (20 cd/m^2). In this set of stimuli, usually only 2 orientations (0, 90) were presented. Red-Green (RG) gratings were generated by modulating red and green guns in counter-phase so that red increase is accompanied with green decrease. Because the peak luminance values for red and green were set equal, the screen was isoluminant and only the color was modulated (100% contrast for both red and green guns). Red Commision Internationale de L'Eclairage (CIE) values were 0.302, 0.545; green CIE values were 0.593, 0.340. Black–white gratings were identical to RG gratings in spatial frequency (SF), temporal frequency, and average screen luminance, but the luminance was modulated at 100% contrast. Thus, for color domain mapping, 4 different gratings (RG horizontal, RG vertical, BW horizontal, BW vertical) were presented to either left eye or right eye, resulting in 8 different stimulus conditions. These 8 conditions plus a blank screen condition (mean luminance 30 cd/m^2) were presented in a randomly interleaved fashion. Because the color signal is a relatively small signal, to minimize the luminance transient, shutters remained open during interstimulus interval and during the blank condition, and eye-specific stimulation was achieved by closing the shutter over the nonstimulated eye (Roe and Ts'o 1995; Landisman and Ts'o 2002a).

Optical Imaging

In one case, an optical chamber was adhered to the skull, filled with silicone oil, and sealed with a glass window. In other cases, the brain was stabilized with agar and images were obtained through a glass cover. Images of reflectance change (intrinsic hemodynamic signals) corresponding to local cortical activity were acquired using either Imager 2001 or Imager 3001 (Optical Imaging Inc., Germantown, NY) with 630-nm illumination (for details see Roe and Ts'o 1995; Ramsden et al. 2001). Signal to noise ratio was enhanced by trial averaging (20–30 trials per stimulus condition) and by synchronization of acquisition with heart rate and respiration. Each stimulus was presented for 3–4 s, during which 15–20 consecutive image frames were taken (4–5 Hz frame rate). Interstimulus interval for all stimuli was at least 8 s. For Imager 2001 system, each frame contains 372 × 240 pixels (representing 8.3 × 6 mm cortex area). For Imager 3001 system, each frame contains 504 × 504 pixels (representing 8 × 8 mm cortex area). Stimuli were presented in blocks of randomly interleaved conditions (see above). Stimulus onset occurred after the first one or 2 frames.

Data Analysis

Single-Condition Maps

For each stimulus condition, we constructed a "single-condition map." The gray value of each pixel in the "single-condition map" represents the percentage change of the light reflectance signal after the stimulus was presented. Specifically, the gray value of each pixel was calculated using following function:

$$\Delta R/R = (F_{5-20} - F_1)$$

in which $\Delta R/R$ represents percentage change, $F_{5\text{-}20}$ is the average raw reflectance values of frames 5–20. F_1 is the raw reflectance value of the first frame (taken before stimulus onset and thus represents the baseline activity). Single-condition maps obtained in this way represent the percentage intrinsic signal change compared with the initial (prestimulus) baseline condition. For stimulus-induced intrinsic signals this is usually a negative value (–0.01% to –0.2%). In single-condition maps, darker pixels represent higher response (more negative) and brighter pixels represent lower response. These maps were then used for calculating differential maps, vector maps (see below), or for further quantification.

Difference Maps (or Subtraction Maps)

All maps for each single condition were summed to increase signal to noise. Pairs of summed maps were then subtracted to reveal preference for one condition versus another. These difference maps were clipped (at 1 standard deviation [SD] from the mean of the pixel distribution) and then normalized to gray level 0–255. Pixel values represent the preference of each pixel to either one of the 2 stimuli: 0 represents strong preference for one condition, 255 represents strong preference for the other condition, and 127 equal response to both. Ocular dominance (OD) maps were obtained by subtracting sum of left eye conditions minus sum of right eye conditions. Orientation maps were obtained by subtracting orthogonal orientation conditions or by vector analysis (see below). Color maps were obtained by subtracting RG and BW conditions (see above). We reasoned that, because all parameters (including spatial frequency, temporal frequency, and mean luminance) were identical for the RG and BW stimuli, any differential response observed must be due to the difference in color content of these 2 stimuli (Roe and Ts'o 1995; Landisman and Ts'o 2002a). Differential signal in color maps tended to be weaker than ocular dominance and orientation maps and usually requires more trials.

Demarcating Functional Domain Locations

To demarcate locations of color domains and orientation domains in V1 and V2, we used 2 methods. In some cases, we threshholded optical images to identify regions most responsive to specific stimuli. With this method, domain selections were based on either single condition (e.g., Fig. 12*C–F*) or difference maps (e.g., Fig. 7*A,D*). To identify regions of maximal response, maps were smoothed (Gaussian filter, 8-pixel

kernel). Low-frequency noise is reduced by convolving the maps with a 150-pixel-diameter circular mean filter, and subtracting the result from the smoothed maps. Resulting maps were then thresholded at the top 10% pixels for color domains (based on the average coverage of CO blobs, see Murphy et al. 1998) or 20% pixels for orientation domains (one out of 4 orientation tested, see Ramsden et al. 2001). Although the precise threshold used affects the domain size, it usually does not affect the domain location. These domain masks were then compared with blood-vessel maps obtained with 570-nm filter (green light); artifacts due to blood-vessel noise were removed. In some cases (e.g., Fig. 8*B*) the thresholding method is not applicable because of the strong noise from blood vessel. In these cases, locations of color domains (the local maximum response location) were identified by centering a 200-μm-diameter spot on the domain; these circular spots were then aligned with other optical maps and with cytochrome-stained sections. Ocular dominance borders were outlined using the thresholding method (e.g., Fig. 4*C,D*).

Calculating Orientation Selectivity

To examine orientation selectivity within V1, we generated orientation vector maps. Single-condition maps of the same orientation were averaged and low-pass filtered (Gaussian filter, 8–15 pixel diameter). Low-frequency noise was removed by convolving this image with a 80- to 120-pixel-diameter mean filter and subtracting the resulting image from the original image. For each pixel, a vector is calculated based on its response to 4 different orientations (vector summation, Bosking et al. 1997). As a result, 2 maps were obtained: the "angle map" representing the orientation preference at each pixel (angles of the vectors) and the "magnitude map" representing the strength of orientation selectivity at each pixel (length of the vectors). The resulting color-coded orientation preference maps and orientation selectivity magnitude maps were then coregistered with color domain locations. From the orientation "angle map," pinwheel locations were also determined by select locations where a continuous shift in orientation preference is observed (Bonhoeffer and Grinvald 1991; Bosking et al. 1997).

Orientation selectivity was quantified for pixels within orientation domains and color blob domains. To evaluate how different these values were from a hypothetical map of unvarying orientation magnitude, we generated orientation magnitude distributions by selecting a number of circular spots (200 μm diameter) at random locations in the V1 (by random selecting of x and y coordinates within blood-vessel–free V1 region where blobs were identified). The number of random locations was determined by averaging the number of blobs and the number of orientation domains within each map. Orientation selectivity of pinwheel locations was determined by averaging 200-μm-diameter regions centered on the pinwheel. For each map, the average pixel value of each of 4 groups (orientation domains, color domains, randomly selected domains, and domains centered on pinwheels) was normalized to the average value of orientation domains and compared using standard t-tests (one-tailed, unpaired equal variance).

Histology and Alignment of CO Staining with Optical Maps

To aide in the alignment of tissue sections and imaged locations, marking lesions were made at selected sites of the cortex either by insertion of a fine gauge needle or with fluorescent markers introduced by inserting a recording tungsten electrode coated with flouroruby. After imaging, animals were given a lethal dose of sodium pentobarbitol and perfused through the heart with 4% paraformaldehyde. Following removal of the brain, the relevant cortical region was removed, the tissue near the lunate was fully unfolded, flattened overnight, and sunk in 30% sucrose solution. The cortical tissue was then sectioned tangentially at 30 μm and reacted for CO histochemistry. To align CO image with optical images, our strategy was to first make the crude alignment based on lesion and tracer injection locations, V1/V2 border location, and V2 stripe location (see Supplemental Fig. 1). We then looked for an alignment of vascular lumen in the cytochrome tissue and points where surface vasculature dives into the cortex and aligned these points with identical points obtained during imaging secession (see Supplemental Fig. 2). This alignment was done in Adobe PhotoShop and involved linear stretch and rotation. However, there are small shifts in the pattern of vascular lumen, either due to actual shifts in traverse or in small distortions in tissue during tissue processing and mounting. Therefore, our final microalignment is guided by considering multiple possible matchings between color and cytochrome patches. Only linear translation, rotation, and scaling of images and tissue sections were performed in alignment.

Results

A total of 5 imaging experiments were performed on 5 hemispheres of 5 adult macaque monkeys. Four imaging cases were performed over medial operculum (representing 5–10° eccentricity) and one case was performed over lateral operculum (representing foveal and perifoveal fields).

Correspondence of Color Blobs to CO Blobs

Case 1

Functional images. For each case, we first obtained the following functional maps: surface blood-vessel map (Fig. 1*A*), which is obtained with illumination of 570 nm (green), ocular dominance map (Fig. 1*B*, OD, subtraction of left eye and right eye), orientation map (Fig. 1*C*, subtraction of 2 orthogonal orientations), and color map (Fig. 1*D*, subtraction of color and luminance gratings). The ocular dominance map (Fig. 1*B*) clearly shows alternating OD stripes in V1 but not in V2, thereby delineating the V1/V2 border (indicated by a short line at right). The orientation map (Fig. 1*C*) shows that both V1 and V2 have strongly activated orientation maps. V2 orientation domains (regions between arrows) are characteristically larger than those in V1 and are separated by zones of poor orientation selectivity (arrows) (Peterhans and von der Heydt 1993; Malach et al. 1994; Roe and Ts'o 1995; Ts'o et al. 2001; Xu et al. 2004).

Figure 1*D* is the color map obtained by subtracting stimulation with isoluminant red/green color gratings and luminance contrast gratings. Because color and luminance gratings contained the same spatial frequency (0.15–0.5 c/deg), temporal frequency (0.5–1 Hz), and average luminance (30 cd/m^2), the only difference between these 2 stimuli is the color content of the stimulus. We considered the possibility that there remained a small luminance contrast difference in the red/green stimuli. However, our examination of high contrast minus low contrast stimuli never revealed any structured maps and never any blob-like pattern (Lu and Roe 2007). Thus, we attribute the differences in activation shown in Figure 1*D* to preferential color response. Dark regions in these maps are areas that have stronger response to color stimuli (or weaker response to luminance stimuli) in comparison with the other regions. In V1, the color map has a striking "blob-like" pattern, reminiscent of CO blob patterns. In V2, the location of the color domains (indicated by arrows in *C* and *D*) colocalizes with regions of poor orientation organization (arrows in *C* and *D*) and is complementary to regions of strong orientation response in V2 (regions between arrowheads in *C* and *D*).

Following the completion of optical imaging we made marking lesions with a fine needle in the cortex (one indicated by white dot in Fig. 1*A*) which produced clearly visible holes in the histological section (one indicated by arrow in Fig. 2*A*). In some cases, we used injections of fluorescent markers (see Supplemental Fig. 1). We first used the lesion and marker locations to get an idea of roughly where in the tissue to look. Then we aligned the large stripes, using thinness and thickness of cytochrome stripes to align to the centers of the nearest color-activated and orientation-activated regions in V2 (see

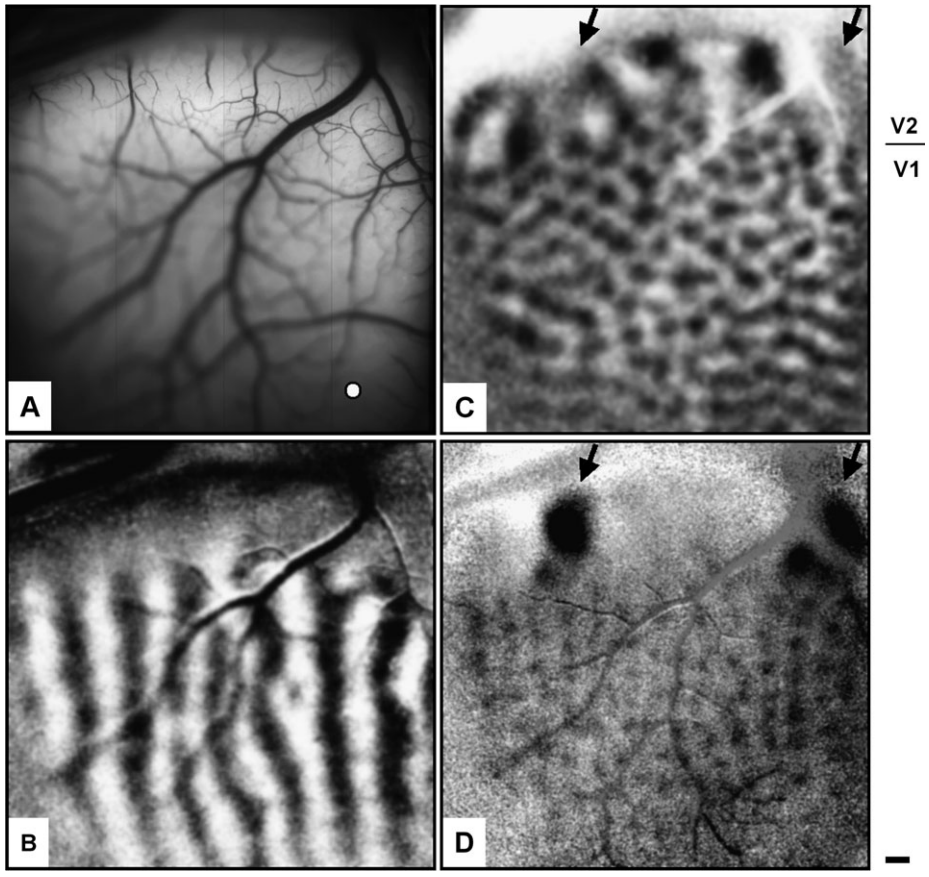

Figure 1. Optical images of functional domains in Macaque V1 and V2. Case 1. (*A*) Blood-vessel map obtained by using green light (570 nm). Lunate sulcus is located at the top. White dot at lower right corner indicates location of marking lesion for later histological alignment. (*B*) Ocular dominance map (left eye minus right eye). V1/V2 border (indicated by short line at right) is demarcated by the lack of ocular dominance columns in V2. (*C*) Orientation preference map (horizontal, dark pixels, minus vertical, light pixels). V2 orientation domains (regions between arrows) are up to several times larger than those of V1. They are complementary to locations of thin stripes (indicated by arrows). (*D*) Color map (red/green isoluminant gratings minus luminance gratings) in which V2 thin stripes (indicated by arrows) and V1 blobs are more activated by the color grating than luminance grating stimuli. Scale bar: 1 mm, applies to (*A*)–(*D*). (Same case as shown in Lu and Roe 2007, Fig. 1).

Fig. 1). The ocular dominance border also served as a guide for approximate alignment. Vessel patterns and CO blobs were then used to do further alignment (see also Supplemental Fig. 2).

V2 stripes. Based on marking lesion locations and the location of the V1/V2 border in both cytochrome and ocular dominance images, we could readily determine a reasonable alignment of CO stripes in V2. In Figure 2*A*, 4 dark stripes, alternating from thin to thick, are visible (arrowheads indicate thick stripes, arrows indicate thin stripes). The location of these stripes aligned well with stripes revealed by general activity (Fig. 2*B*, sum of all SF = 0.21 c/deg conditions minus blank condition). Furthermore, thin stripes identified by cytochrome (arrows in Fig. 2*A*) coaligned with color stripes identified with optical imaging (arrows in Fig. 2*D*) and with regions of poor orientation selectivity (arrows in Fig. 1*C*). Pale and thick (arrowheads in Fig. 2*A*) stripes identified by cytochrome coaligned with regions of orientation domains identified by optical imaging (Fig. 1*C*). This clearly demonstrates that thin stripes in V2 are regions of preferential color activation and poor orientation selectivity (at least at population level), and that thick/pale stripes are regions of higher orientation selectivity and relatively poorer color response. Consistent with previous findings (Roe and Ts'o 1995; Xiao et al. 2003; Wang et al. 2007), thin stripes contain color-preferring regions (black spots).

V1 blobs. We examined alignment of color-activated domains in V1 with CO-stained blobs. Figure 2*C*, *D* illustrates the CO-stained tissue (*C*) and corresponding imaged tissue (*D*). Typically, with long periods of recording and unfolding of tissue near the lunate, there is some distortion of the tissue and therefore alignment often is not exact. However, one can align relatively large portions of the tissue at a time. In Figure 2*E*, *F*, we have focused on the central portion of the tissue and illustrated this alignment. Guided by alignment of V2 stripes, lesion spots, the V1/V2 border, and blood vessels, we found a reasonable alignment of color blobs with CO blobs. In Figure 2*E*, *F*, some of the matching blobs are indicated (small white arrows). As long recording periods lead to some swelling of the cortical tissue, we have biased the alignment toward the center of the field (shown enlarged in *G* and *H*). Note that the color domains are remarkably similar to the cytochrome blobs with respect to both size and spacing. There are a large number of closely matching blobs throughout the center of the image. However, not all blobs align exactly. There are locations of cytochrome staining with weak color activation and locations of apparent color activation with weak cytochrome staining. Factors that may contribute to apparent mismatches include tissue distortion during histological processing, unevenness of cytochrome staining, and local differences in signal/noise during imaging. However, overall, considering the distortion during

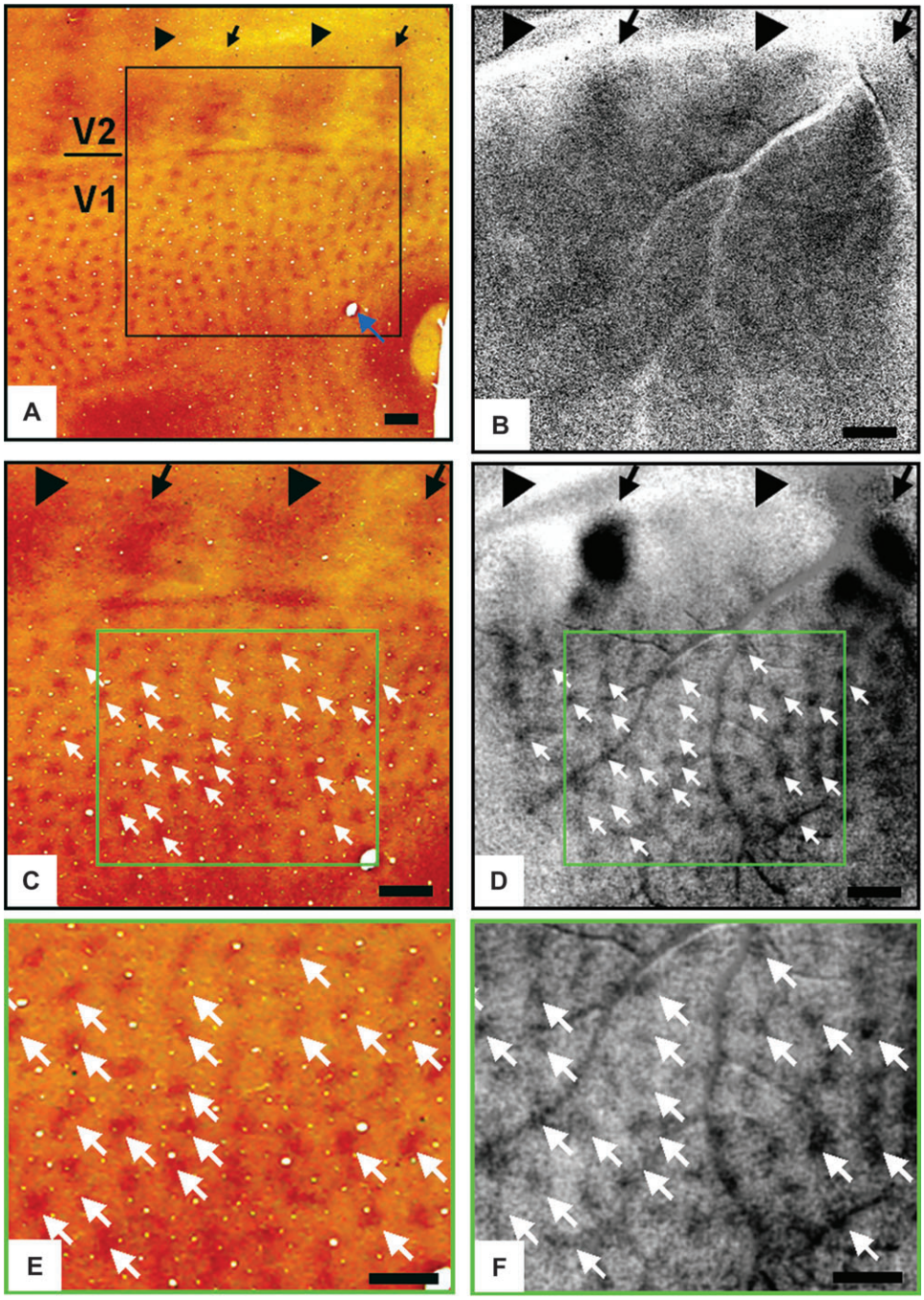

Figure 2. Alignment of CO staining with imaged color domains. Case 1. CO sections are shown in left column. Maps obtained with optical imaging are shown in right column. (*A*) Large field view of CO section containing imaged cortical region (black frame) shown in Figure 1. Tissue underlying lunate sulcus (very top of image) has been opened and flattened. Thin and thick stripes are indicated by arrows and arrowheads, respectively. One needle lesion location is indicated by small blue arrow at lower right corner (white dot in Fig. 1*A*). Border between V1 and V2 is also indicated. (*B–F*) Field of view is the same as framed area shown in (*A*). (*B*) General activity map stimulated by low-frequency gratings (generated by summing all SF = 0.21 c/deg stimulus conditions minus blank condition). Dark activation stripes in V2 align with CO dark stripes in (*A*) (arrows and arrowheads at top). (*C*) Cytochrome-stained section with small white arrows point to blobs in central portion of imaged region. (*D*) Color map (same as Fig. 1*D*) illustrating alignment of color blobs in V1 with CO blobs (small arrows from (*C*) are superimposed) and color-activated stripes in V2 with thin CO stripes (arrows at top). (*E*, *F*) Enlarged views of green framed areas in (*C*) and (*D*). Scale bars: 1 mm.

tissue processing, the high number of match points, and the specificity of the pattern and spacings of blobs, these color domains and cytochrome blobs exhibit a remarkably good match. We compared these matches with possible random effects (i.e., matching 2 totally random sets of points). We found that the matches between color blobs and CO blobs are highly significantly from random in terms of average density (*t*-test $P < 0.05$) and average center–center distance (*t*-test, $P < 0.002$).

Case 2

Functional images of lateral operculum. Figure 3 shows optical images from a second case (8 × 8 mm field of view).

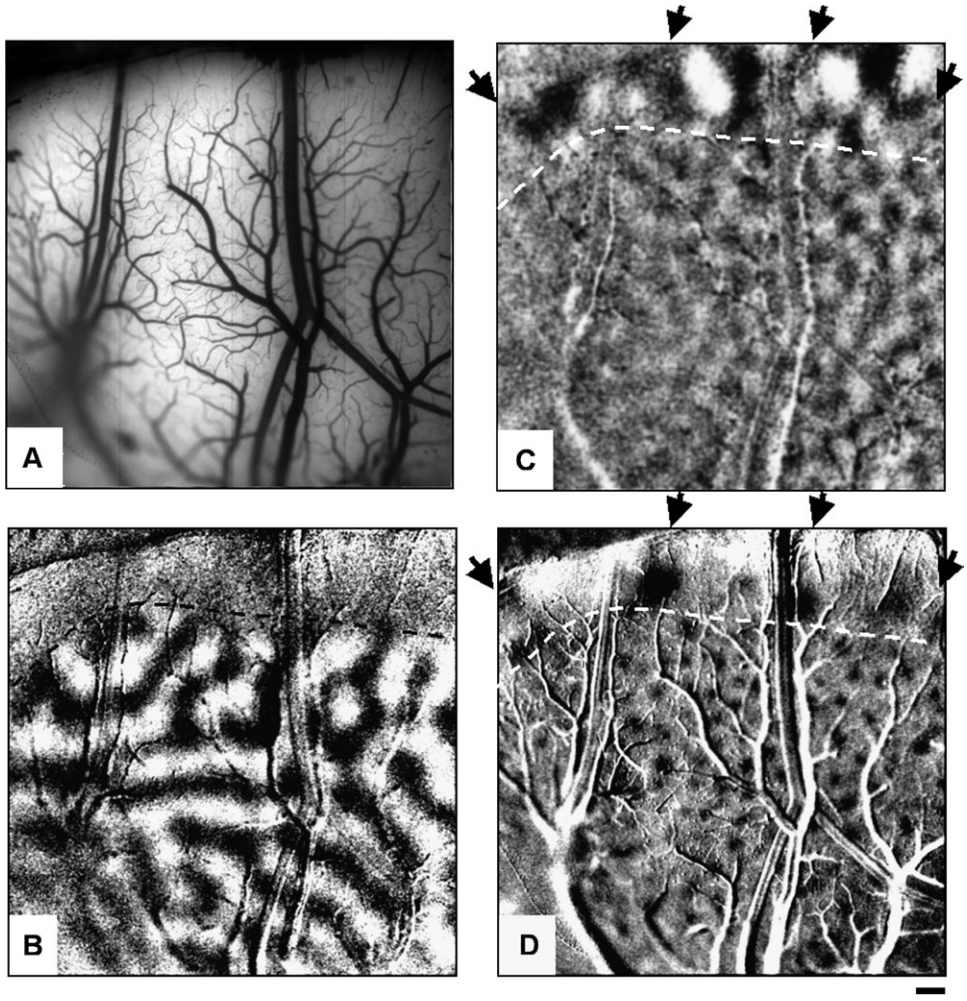

Figure 3. Optical images of functional domains in Macaque V1 and V2. Case 2. (*A*) Blood-vessel map. Lunate sulcus is located at the top. (*B*) Ocular dominance map (left eye minus right eye). V1/V2 border indicated by dotted line. (*C*) Orientation map (horizontal minus vertical). V2 orientation domains are up to several times larger than those of V1. V2 orientation domain locations are complementary to locations of thin stripes (arrows). (*D*) Color map in which V2 thin stripes and V1 blobs are more activated by the color grating than luminance grating stimuli. Arrows indicated locations of thin stripes in V2. Scale bar: 1 mm, applies to (*A*)–(*D*).

The layout is the same as in Figure 1. Figure 3*A* is the blood-vessel pattern with the lunate sulcus located at the top of the image. Note the curvature of the V1/V2 border at this lateral extreme of the operculum which represents central visual field. Although the image clearly shows alternating OD stripes in V1, the ocular dominance pattern is more irregular and differs from the common pattern of parallel columns. We believe this is probably due to the lateral location of the imaged region as we have never seen such a pattern in more medial locations (representing 5–10°) of the operculum (cf. Horton and Hocking 1996). The orientation map (Fig. 1*C*, horizontal–vertical) has a typical, 200- to 300-μm-sized orientation domain in V1 and domains in V2 that are 2–3 times larger. As shown previously, regions of strong orientation selectivity in V2 are separated by zones of poor orientation selectivity (arrows) (Peterhans and von der Heydt 1993; Malach et al. 1994; Roe and Ts'o 1995; Ts'o et al. 2001; Xu et al. 2004). The color map (shown in Fig. 3*D*) in V1 bears the striking "blob-like" pattern seen in CO blob patterns. In V2, regions of dark activation (indicated by arrows) occur at intervals consistent with the spacing of thin stripes and colocalizes with regions of poor orientation organization in V2 (compare *C* and *D*).

Alignment of cytochrome pattern and functional images. Figures 4 and 5 show alignment of CO-stained tissue and optical images from this case. In this case, a large tear in the cortex (indicated by asterisk in Fig. 4*A*) obscures clear demarcation of the V2 stripes and the V1/V2 border. However, using the tracer markers and blood-vessel patterns as guides, we were able to align the tissue over V1. Figure 4*A* is a superficial section of the tissue in which the outlines of large surface blood-vessel patterns are visible, making the alignment of the optical image of vascular pattern relatively straightforward (Fig. 4*B*). In this case, microinjections of fluorescent tracer were also made at several cortical locations (Fig. 4*B*, red dots) to further aid in alignment of images with tissue. The inset at the lower right corner of Figure 4*B* illustrates visualization of one of the fluorescent tracer injection sites (see also Supplemental Fig. 1). Figure 4*C* illustrates the region of the tissue corresponding to the imaged field of view, taken from a slightly deeper section (approximately 400 μm from the surface). The ocular dominance pattern (Fig. 4*D*, same as Fig. 3*B*) is superimposed on the CO pattern (Fig. 4*C*). One of the characteristics of CO blobs is that they tend to align along the centers of ocular dominance columns (Horton 1984). This overlay shows that, despite the

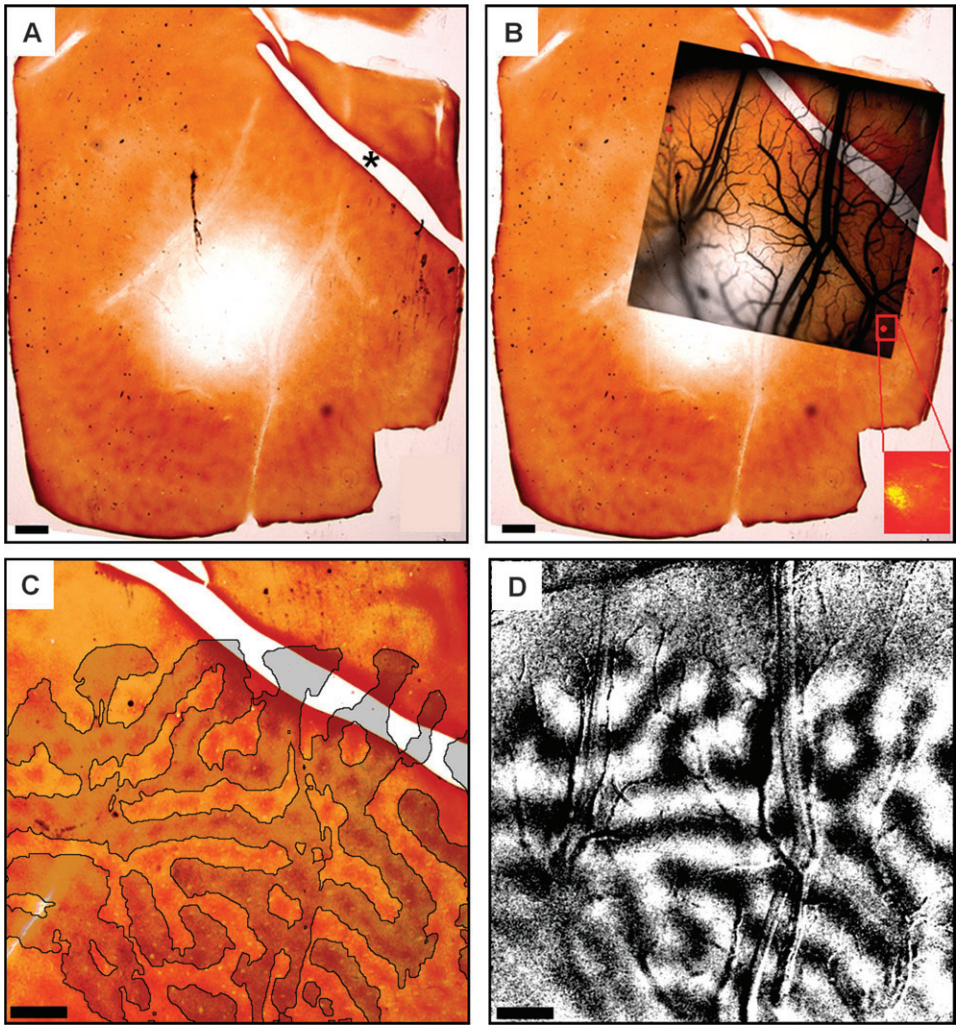

Figure 4. Alignment of CO pattern with imaged ocular dominance maps. Case 2. (*A*) Large field view of CO section containing imaged cortical region in Figure 3. This is one of the top layers containing visible vessel patterns. Tissue underlying lunate sulcus (very top of image) has been opened and flattened. The large break in tissue (asterisk) is a tear in the tissue. (*B*) Alignment of imaged blood-vessel map with tissue. Blood-vessel patterns were aligned. Fluorescent tracer injection locations (red dots) were also used as initial crude alignment guides. Inset illustrates one of the fluorescent tracer injection sites (see Supplemental Fig. S1). (*C*) Cytochrome stained section overlaid with ocular dominance mask (from *D*) which shows that CO blobs are aligned along center of ocular dominance stripes. CO section is from approximately 400-μm depth which shows blob pattern. Field of view is the same as vessel map shown in (*B*). In this case, the tear in tissue has prevented good staining of stripe structure in V2. (*D*) Ocular dominance (OD) map (left eye minus right eye), same as in Figure 3*B*. Scale bars: 1 mm.

irregularity of ocular dominance pattern, most CO blobs lie on the center of either left eye or right eye stripes. The match of CO pattern and ocular dominance pattern also provides additional confirmation (beside blood vessel, fluorescent marker) of the good alignment between histological maps (CO) and functional maps.

This alignment enabled the comparison of the CO blobs (Fig. 5*A*, same CO section as Fig. 4*C*) and the color-activated domains in V1 (Fig. 5*B*). In a higher magnification view (Fig. 5*C,D*), the green arrows indicate that the blobs appeared to correspond reasonably well. We observed that, in this case, whereas color activation spots appeared focal, CO blobs were often elongated and exhibited frequent "bridges" (cf. Ts'o and Gilbert 1988; Landisman and Ts'o 2002a, 2002b). However, detailed examination of the cytochrome blob pattern and the color map reveal a striking correspondence (compare green arrows in Fig. 5*C,D*). Dark pixels in the color map tend to correspond with dark cytochrome staining and not with cytochrome light areas. Note that not every CO blob has a corresponding color blob in the color-luminance map. Some color blob activations may be obscured or weakened by blood-vessels noise. This may also suggest that in some cases color activation comprise only a portion of the cytochrome dark regions. It is unclear whether this may be an eccentricity related effect.

To further examine the correspondence between color blobs and CO blobs, we calculated 2 average blob maps: 1) average color blob maps and 2) average CO blob maps using color blob coordinates. The averaged color blob map from case 1 is illustrated in Figure 6*A*. It is a simple average of all color blobs patches in Figure 2*D* (2 × 2 mm, $N = 63$) aligned at color blob centers. Figure 6*B* is calculated from the CO-stained tissue (i.e., Fig. 2*C*) but using the *x*–*y* position of color blobs. Note that this is not a simple average of CO blobs, instead, it represents a 2-dimentional spatial cross-correlation of the CO and color maps. The darkness of this map at each position corresponds to the average CO-staining density at each distance from the average color blob coordinates. If the relative locations of color blobs and CO blobs are random, the cross-correlation map (Fig. 6*B*)

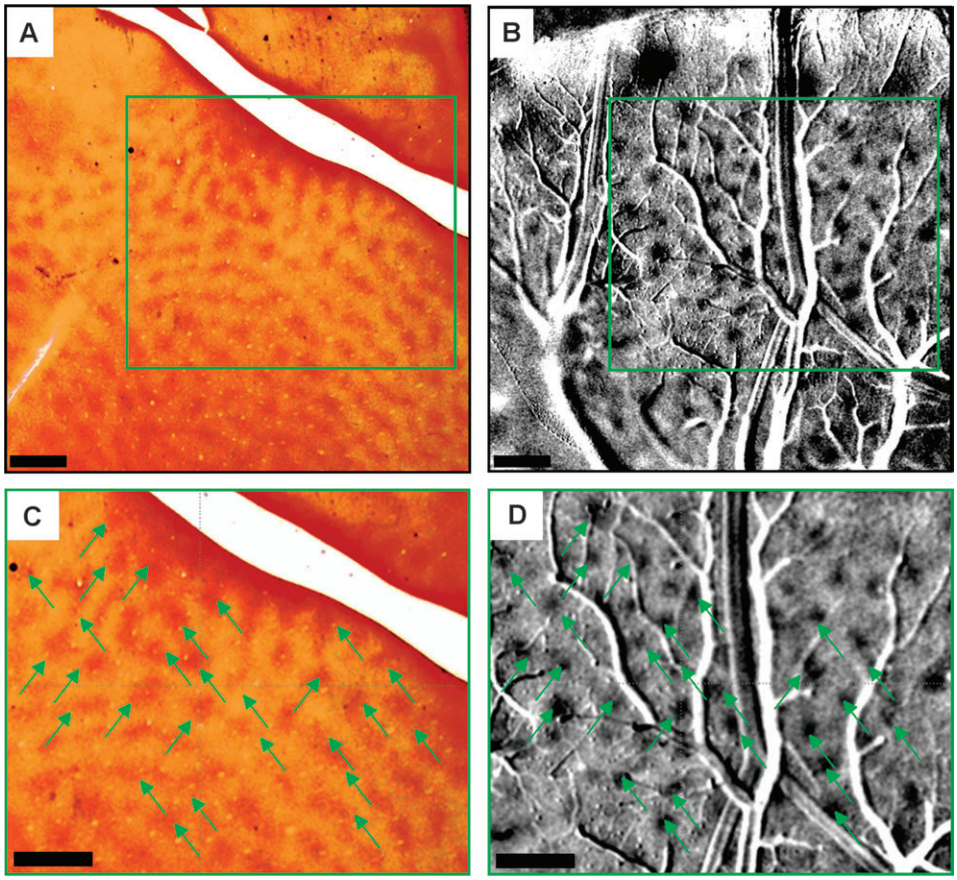

Figure 5. Alignment of CO blobs with imaged color domains. Case 2. (*A*) The same CO section as shown in Figure 4*C* in which green framed area is enlarged below in (*C*). (*B*) Color map showing blobby pattern in V1 and patches of color domains in V2 (same as Fig. 3*D*). (*C* and *D*) Enlarged views of framed areas in (*A*) and (*B*). Green arrows point to corresponding cytochrome blobs and color blobs. Scale bars: 1 mm.

would be homogenous. However, what we observe is a dark peak near the center of the image, indicating that color blobs and CO blobs are spatially correlated.

To depict this graphically, the 2-dimensional "single-blob" maps in Figure 6*A,B* were collapsed radially onto a single dimension based on averaged pixel values on a ring centered at middle and at different radii (0–1 mm). This gives the plot shown in Figure 6*C*, where the average pixel values in both maps (color and CO maps) were normalized and plotted as functions of distance from the center. Only values from radius 0 to 1 mm were available, but the curves were copied symmetrically to give a more intuitive look. Curves for both color blobs and CO blobs share a similar shape: peak at center, half-height width around 200 μm, lowest density at around 300 μm, and a second peak at around 600–650 μm, which represents neighboring blobs. The similarity of these 2 curves provides further evidence that these 2 sets of blobs are highly overlapping.

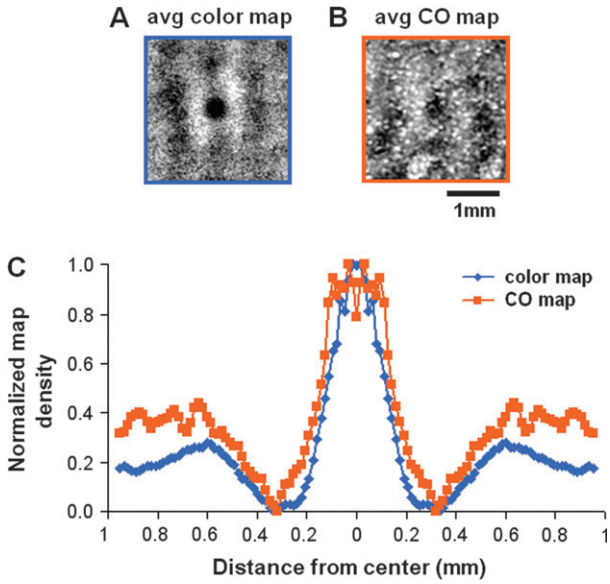

Figure 6. Overlap between average color blob and average CO blob. (*A*) The average color blob obtained by summing 60.2 mm × 2 mm regions centered on 60 color blobs. (*B*) The average CO blob obtained by summing 60 regions (2×2 mm) centered on the same set of 60 coordinates for color blobs. (*C*) Radially compressed density profile of the average color blob (blue) and the average CO blob centered on color blob coordinates (orange). Numbers on *x* axis indicate distance from center of the average blob. The color and CO profiles are very similar, indicating a high degree of overlap between color blobs and CO blobs.

Alignment with Centers of Ocular Dominance Columns

Previous studies have shown that CO blobs tend to align along the center of imaged ocular dominance columns. If imaged color blobs do align with CO blobs, they should also align along the center of ocular dominance columns. In previous studies, it has been shown that cells in blobs are predominantly monocular (Livingstone and Hubel 1984) and that centers of monocularity align well with CO blobs (Ts'o et al. 1990; Vnek et al. 1999;

Landisman and Ts'o 2002a). However, imaged color-activated blobs have been reported to bear only a loose association with ocular dominance maps (Landisman and Ts'o 2002a). Here, we have re-examined this issue. As shown by Figures 7 and 8, we find that both these predictions are met.

Figure 7 illustrates the overlay of the color domains (color map in Fig. 7*A*, thresholded outlines in Fig. 7*B*) on the ocular dominance map (Fig. 7*D*) of case 1. Examination of Figure 7*D* reveals that the color-activated domains align along both the left eye (dark pixels) and right eye (light pixels) ocular dominance

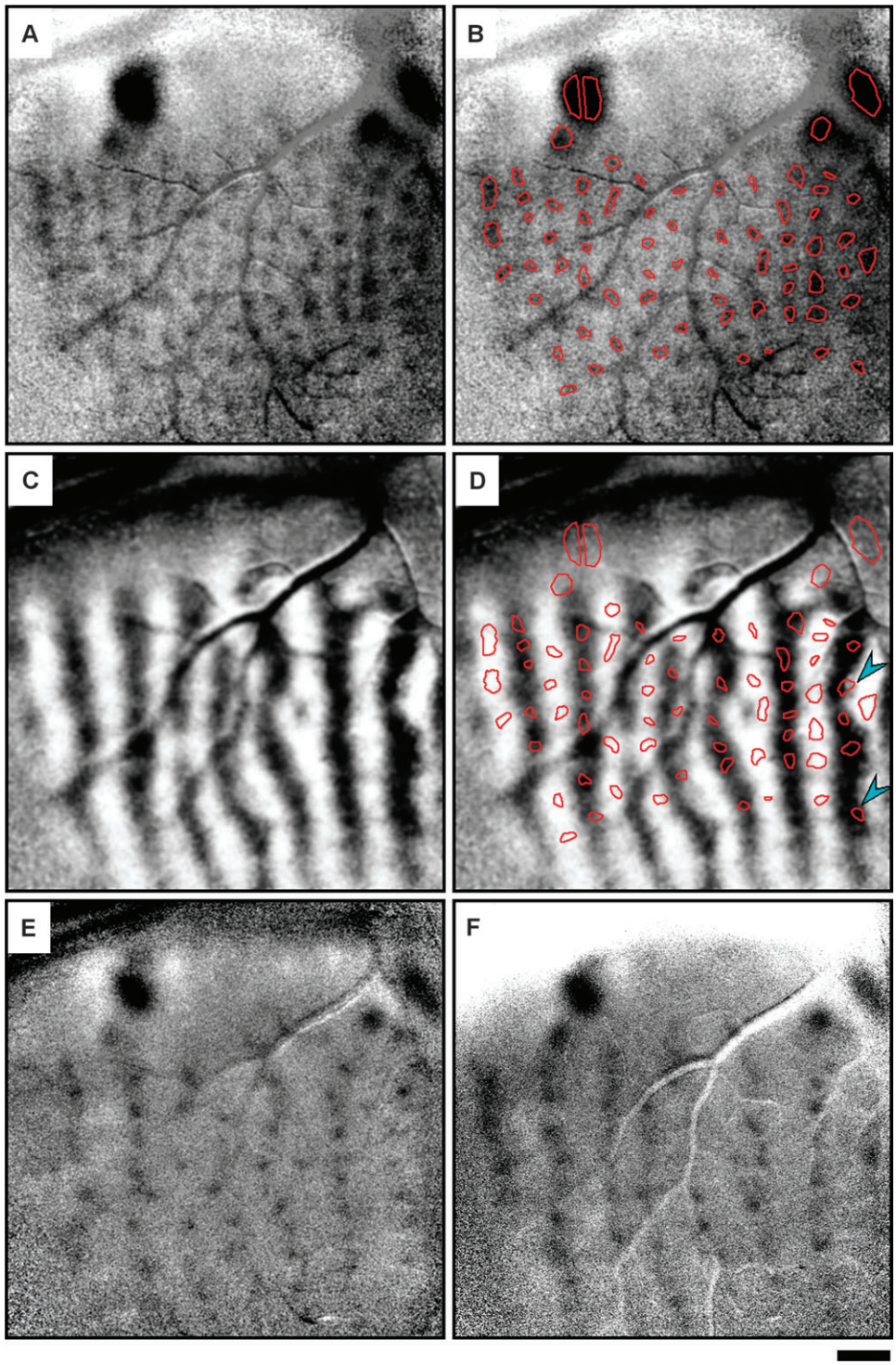

Figure 7. Alignment of color blobs along ocular dominance columns. Case 1. (*A*) Color map of V1 and V2. Same as map shown in Figure 1*D*. (*B*) Color map with mask of thresholded color blobs overlain (red outlines). (*C*) Ocular dominance map (left eye minus right eye). (*D*) Ocular dominance map with color blob mask overlay. Color blobs tend to align along center of ocular dominance columns in V1. Arrowheads: 2 color blobs on or near ocular dominance borders. (*E*) Color map from left eye stimulation (RG left eye—BW left eye) which shows color blobs at left eye monocular zones. (*F*) Color map from right eye stimulation (RG right eye—BW right eye) which shows color blobs at right eye monocular zones. Scale bar: 1 mm, applies to (*A*)–(*D*).

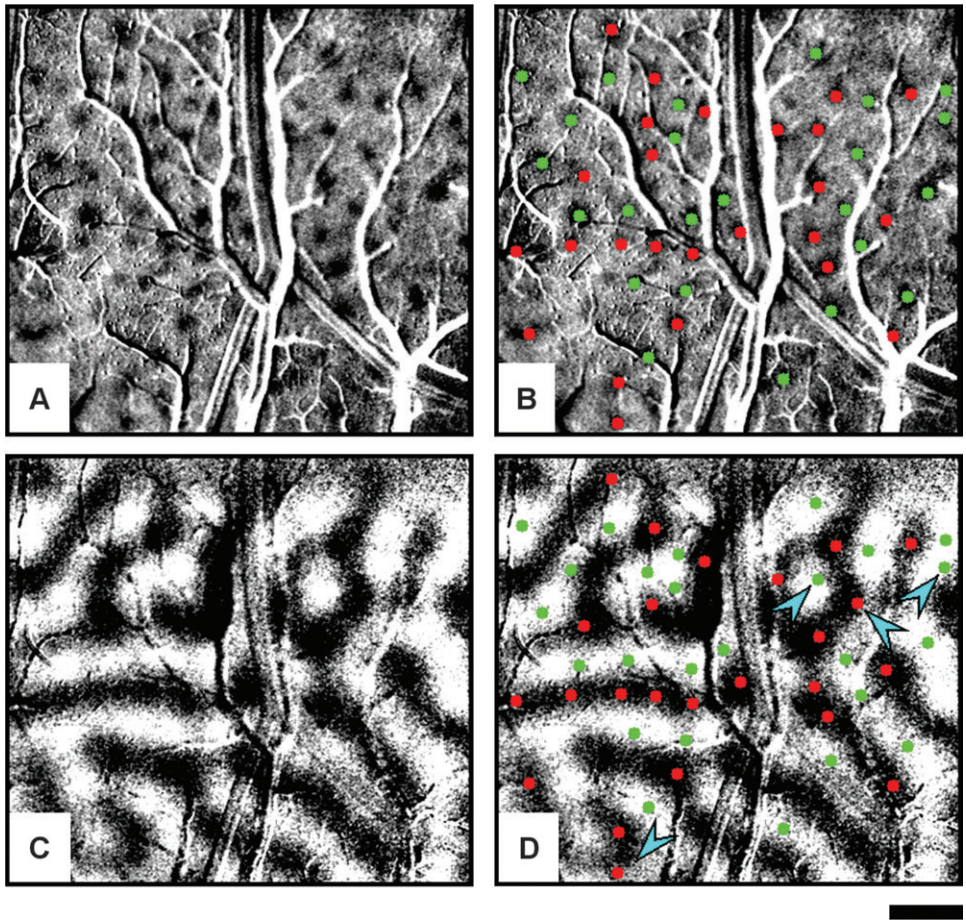

Figure 8. Alignment of color blobs along ocular dominance columns. Case 2. (*A*) Color map, from V1 portion of Figure 3*D*. (*B*) Color map with color blobs marked by red (left eye) and green (right eye) dots. (*C*) Ocular dominance map (left eye minus right eye). (*D*) Ocular dominance maps with color dot overlay. Color blobs tend to align along center of ocular dominance columns. Arrowheads indicate color blobs on or near ocular dominance borders. Scale bar: 1 mm, applies to (*A*)–(*D*).

columns. Of the encircled 63 V1 color domains, only 2 (indicated by blue arrowheads) fall toward or on an ocular dominance border; the remaining 61 lie within single ocular dominance column. However, note that the match between cytochrome blob patterns and ocular dominance is not 100% either (Horton 1984; Landisman and Ts'o 2002a). Figure 7*E*, *F* shows color activation map from monocular stimulation. Figure 7*E* (RG left eye minus BW left eye) shows color blobs aligned in the center of left eye columns, whereas Figure 7*F* (RG right eye minus BW right eye) shows color blobs aligned in the center of right eye columns. Thus, we do not find any evidence for merging of blob pairs across ocular dominance borders when color maps from the left and right eyes are summed (cf. Landisman and Ts'o 2002a). Also note that the color center in Figure 7*E*, *F* is identical to the blobs in Figure 7*D*, and thus also aligned in the center of ocular dominance columns. Together, Figures 2 and 7*E*, *F* clearly demonstrate that 1) blobs are more strongly driven by monocular stimulation than interblob regions and 2) blobs are preferentially activated by color stimuli. Furthermore, color ocular dominance columns (left eye color, right eye color) have a blob-like appearance, and are quite distinct from the typical stripe-like ocular dominance pattern. Both the functional characteristics of these color domains and their spatial relationship to ocular dominance patterns support the correspondence of color blobs with CO blobs.

The typical ocular dominance pattern has borders running perpendicular to the V1/V2 border. However, previous reports have illustrated great variation in the patterns of ocular dominance (Horton and Hocking 1996). We have also observed this in some cases. In case 2, we observed ocular dominance columns with a more irregular pattern (Fig. 8*C*, *D*). In this case (same case as in Fig. 3), we imaged very central visual fields (lateral operculum). Here, the V1/V2 border begins to turn caudally as it approaches the end of the lunate sulcus (see Fig. 3*B*). Although the columns continue to run orthogonal at the V1/V2 border, due to the turning of the V1/V2 border, the pattern away from the border becomes more irregular and tortuous. We wanted to examine whether at this eccentricity color blobs would still lie along centers of ocular dominance columns. The color map in this case is shown in Figure 8*A*, which reveals a blob-like pattern in V1. The color blobs are indicated by dots in Figure 8*B*. When this dot pattern is overlain on the ocular dominance map (Fig. 8*D*), it is again apparent that the color blobs fall along ocular dominance centers. In this case, 4 out of 49 color blobs fall at or near ocular dominance borders (indicated by arrowheads).

Figure 9 is an additional case (case 3) that illustrates this point. The color map in this case is somewhat noisier. However, the tendency for color blobs to fall within ocular dominance columns and not at borders between columns is still apparent.

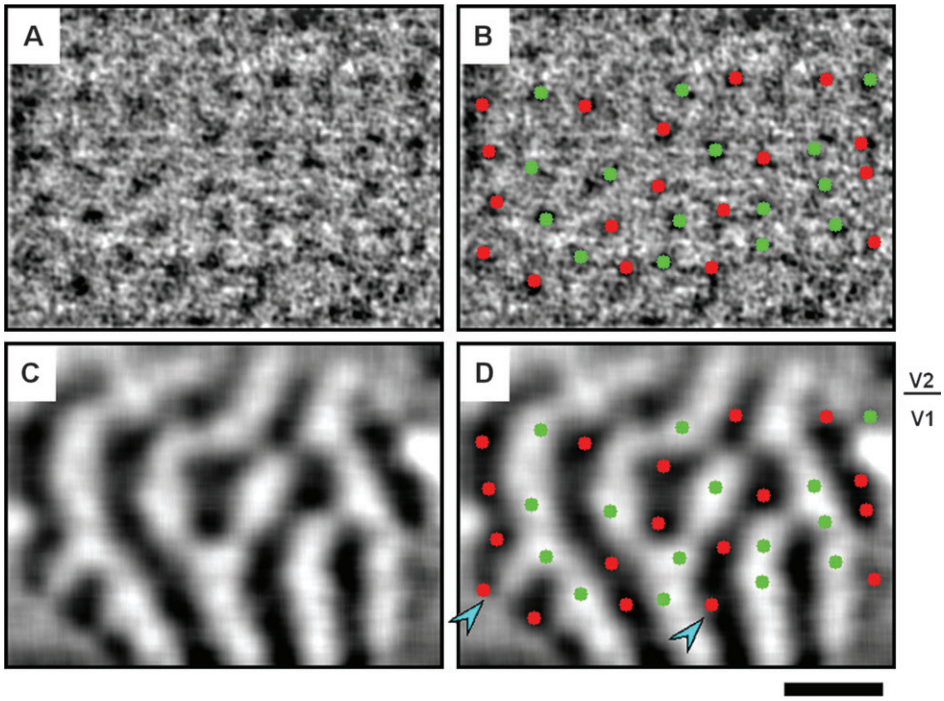

Figure 9. Alignment of color blobs along ocular dominance columns. Case 3 (in this case, a 1.25 c/deg thin white line grating was used for obtaining OD and orientation maps). (*A*) Color map of V1 in which V1 blobs are more activated by the color grating than luminance grating stimuli. (*B*) Color map with color blob positions marked by red (left eye) and green (right eye) dots. (*C*) Ocular dominance map (left eye minus right eye). (*D*) Ocular dominance maps with color blob location overlay. Color blobs tend to fall along center of ocular dominance columns. Arrow heads: color blobs on or near ocular dominance borders. Scale bar: 1 mm applies to (*A*)–(*D*).

In this case, 2 out of 35 marked domains fell on or near ocular dominance borders (indicated by arrowheads). In all the cases we examined, most blobs fall in or near the center of ocular dominance columns; some cases show this tendency more strongly than others. The average OD width of these 3 cases is 450.4 μm. The average blob-center to OD-center distance is 44.7 ± 53.4 μm (SD) which is significantly shorter than the average distance of randomly selected points to the OD center (112.7 ± 76.7 μm, *t*-test, $P < 0.0001$).

Color Domains Do Not Coincide with Orientation Domains in V1 and V2

There is controversy as to whether blobs in V1 are less orientation-selective than interblobs. The original modified ice cube model illustrated blobs as pegs in the center of a hypercolumn (Horton 1984; Livingstone and Hubel 1984). However, Landisman and Ts'o (2002a) report that there is only a loose association between color selectivity and orientation. We now present evidence for a stronger "negative" association, one which is consistent with the original Livingstone/Hubel model. Figure 10 is the same case shown in Figure 1. Figure 10*A* shows the color domain mask (red outlines) overlaid on the color map. These color domains were overlain on the 0° minus 90° (Fig. 10*B*) and the 45° minus 135° (Fig. 10*C*) orientation domain maps. The red outlined color domains do not consistently coincide with either the dark 0° orientation domains (Fig. 10*B*, dark pixels) or the 90° orientation domains (Fig. 10*B*, light pixels). Neither do they coincide with the 45° orientation domains (Fig. 10*C*, dark pixels) or the 135° orientation domains (Fig. 10*C*, light pixels). This minimal overlap between the color and orientation domains is further demonstrated in Figure 10*D*, *E*. Figure 10*D* shows horizontal (blue outlines) and vertical (green outlines) orientation domain masks overlain on the orientation map. When the color mask (red) is overlain on the orientation masks (green) there is little overlap (Fig. 10*E*). These overlays illustrate that the color domains typically do not coincide with centers of orientation domains (cf. Bartfeld and Grinvald 1992; Landisman and Ts'o 2002a).

This point is illustrated also by a second case (case 4) shown in Figure 11. In this case, the ocular dominance map is shown in Figure 11*B*. The V1/V2 border is at the top (outside of the field of view). The orientation map (horizontal minus vertical) is shown in Figure 11*C*, *D*. In Figure 11*D*, horizontal domains (blue outlines) and vertical domains (green outlines) were superimposed. The color map in Figure 11*E*, *F* reveals blobs in V1. Overlay of color and orientation domains (Fig. 11*G*) illustrates that color domains do not coincide with centers of orientation domains.

Figure 12 illustrates a third case (case 3, same case as Fig. 9). The centers of color blobs (Fig. 12*A*, red dots) are overlain on the color-coded orientation map shown in Figure 12*B*. The lack of overlap with domains of any single orientation is illustrated in Figure 12*C*–*F*. These 4 color maps are thresholded maps of single-condition orientation maps. The red dots tend not to coincide with centers of 0° (Fig. 12*C*), 45° (Fig. 12*D*), 90° (Fig. 12*E*), or 135° (Fig. 12*F*) orientation domains.

Note that there are a comparable number of blobs and orientation domains. For example, in Figure 10, within regions in which reasonable color imaging was obtained (rectangular in Fig. 10*E*), there are approximately 62 blobs (red), 57 horizontal domains (blue), and 46 vertical domains (green). In Figure 11, within the region within which reasonable vessel-free color imaging was obtained (rectangular Fig. 11*G*), there are approximately 18 blobs (red), 20 horizontal domains (blue), and 25

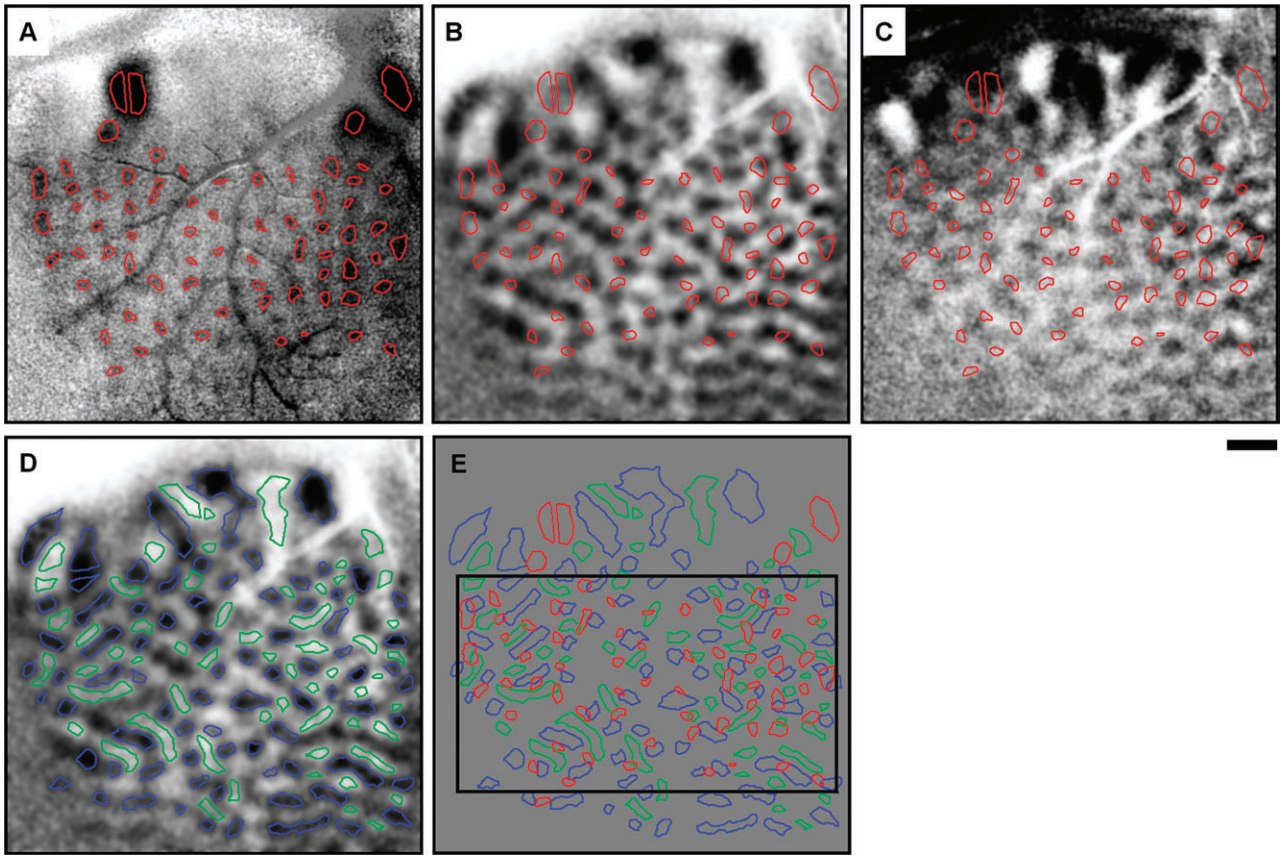

Figure 10. Blobs do not coincide with centers of orientation domains, case 1. (*A*) Color domain mask (red) overlaid on the color-luminance map (same as in Fig. 1*D*) identifies blobs in V1 and thin stripes in V2. (*B*) Color domain mask (red) overlaid on the 0–90 (HV) orientation map. (*C*) Color domain mask (red) overlaid on the 45–135 (AO) orientation map. (*D*) Horizontal (blue) and vertical (green) orientation masks overlaid on the HV orientation map. (*E*) The overlay of HV orientation domain masks and color domain mask. There is little overlap between orientation and color domains. Rectangle indicates region from which blob and orientation domain counts were obtained (see text). Scale bar: 1 mm, applies to (*A*)–(*E*).

vertical domains (green). In Figure 12, the ratios of color domains and orientation domains of a single orientation preference are also comparable. The numbers of domains counted are influenced by variability of signal strength across a field of view, differences in signal strength between color domains and orientation domains, distinctness of domains (e.g., color blobs appear focal whereas orientation domains often appear elongated), and vessel artifacts. Despite these factors, the number of blobs and the number of domains of a single orientation preference are not tremendously different. These numbers may be consistent with a ratio of a single color blob to a full cycle of orientation columns.

Color-Activated Blobs are Regions of Low Orientation Selectivity

To further evaluate the locations of color blobs, we examined their relationship to orientation selectivity in V1 more quantitatively. We calculated at each pixel the direction and magnitude of orientation response, resulting in the orientation angle map (Fig. 12*B*) and the orientation selectivity magnitude map (Fig. 12*G*). Scrutiny of the registration in Figure 12*G* reveals that blobs tend to coincide with regions of low orientation selectivity (the red crosses tend to overlie black pixels). We further compared the average pixel values (from Fig. 12*G*) from orientation domains (normalized to 1) and other domain types (color blobs, random selections, and pinwheels) by selecting circular regions centered at domain centers and having a diameter of 200 μm. The mean value of orientation selectivity of the blobs ($\overline{x}$=0.53±0.25) is significantly lower ($P < 0.001$) than that of orientation domains ($\overline{x}$=1±0.27) (Fig. 12*H*). Each of these values is significantly different from the orientation selectivity of circular regions chosen at random ($\overline{x}$=0.75±0.29) (for calculation of random, see Methods). This indicates that the orientation selectivity of orientation domains is greater than what would be expected from a random selection of pixel. The orientation selectivity of blobs, in contrast, is less than what would be expected from a random selection of pixels. We also examined the magnitude of orientation selectivity at pinwheel centers, which is lowest among all these groups ($\overline{x}$=0.40±0.1, $P < 0.001$ compare with blobs, Fig. 12*H*).

To further illustrate this point, 2 additional cases are shown in Figures 13 (case 1) and 14 (case 5). The color maps are shown in Figures 13*A* and 14*A*, orientation angle maps in Figures 13*B* and 14*C*, and the orientation selectivity magnitude maps in Figures 13*C* and 14*D*. For each of these cases, quantification revealed significantly lower mean orientation selectivity of color blobs (Fig. 13*D*: $\overline{x}$=0.70±0.39, Fig. 14*E*: $\overline{x}$=0.46±0.17) than orientation domains (Fig. 13*D*: $\overline{x}$=1±0.38, Fig. 14*E*: $\overline{x}$=1±0.24). Each of these values was significantly different from the orientation selectivity of pixels chosen at random (Fig. 13*D*: $\overline{x}$=0.82±0.39, Fig. 14*E*: $\overline{x}$=0.64±0.71), again indicating that the orientation selectivity of orientation domains is greater than what would be expected

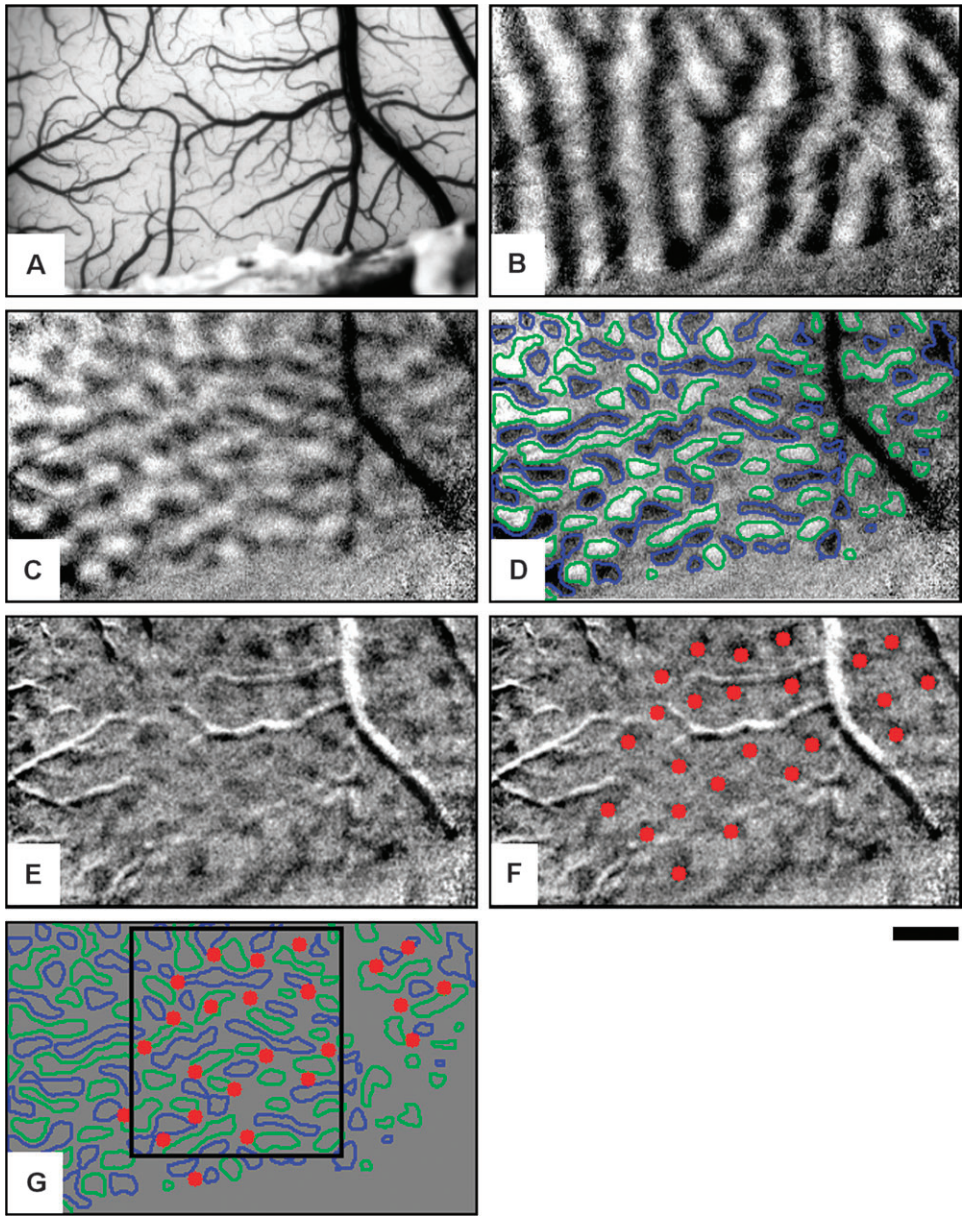

Figure 11. Blobs do not coincide with centers of orientation domains, case 4. (*A*) Blood-vessel map. (*B*) Ocular dominance map (left eye minus right eye). Lunate is at the top (outside of the field of view). (*C*) Orientation map (horizontal minus vertical). (*D*) Horizontal minus vertical orientation map with horizontal domains marked by blue outlines and vertical domains marked by green outlines. (*E*) Color map in which V1 blobs are more activated by the color grating than luminance grating stimuli. (*F*) Blob locations are marked with red dots. (*G*) Overlay of color blob (red), horizontal domain (blue), and vertical domain (green). There is little overlap between these domains. Rectangle indicates region from which blob and orientation domain counts were obtained (see text). Scale bar: 1 mm apply to (*A*)–(*G*).

from a random selection of pixels and that of blobs is less than what would be expected from a random selection of pixels.

In the cases shown in Figures 12–14, we also examined orientation selectivity at pinwheel regions. As expected, pinwheels are also locations of low orientation selectivity (Maldonado et al. 1997; Schummers et al. 2002; Ohki et al. 2006). The orientation selectivity of pinwheels (Fig. 12*H*: $\overline{x}$=0.4±0.1, Fig. 13*D*: $\overline{x}$=0.54±0.2, Fig. 14*E*: $\overline{x}$=0.39±0.11) in these cases was significantly lower than those of the color blobs. This significant difference suggests that pinwheels and blobs are not the same structures, consistent with previous findings that positions of blobs and pinwheel centers do not have a high correlation (Bartfeld and Grinvald 1992; Blasdel 1992a, 1992b).

Discussion

Summary

In V1, we find that color responsive domains exhibit an appearance similar to that of CO blobs. Color domains appear focal, measure ~200–250 μm in size, and are similar in density and spacing to cytochrome blobs. Furthermore, color domains tend to align along ocular dominance columns and coincide with centers of monocularity. We find this both in perifoveal and foveal regions of V1. Whereas ocular dominance maps in V1 have a columnar appearance, color ocular dominance maps in V1 have a blobby appearance. We find that color domains do not coincide with centers of orientation domains and exhibit low

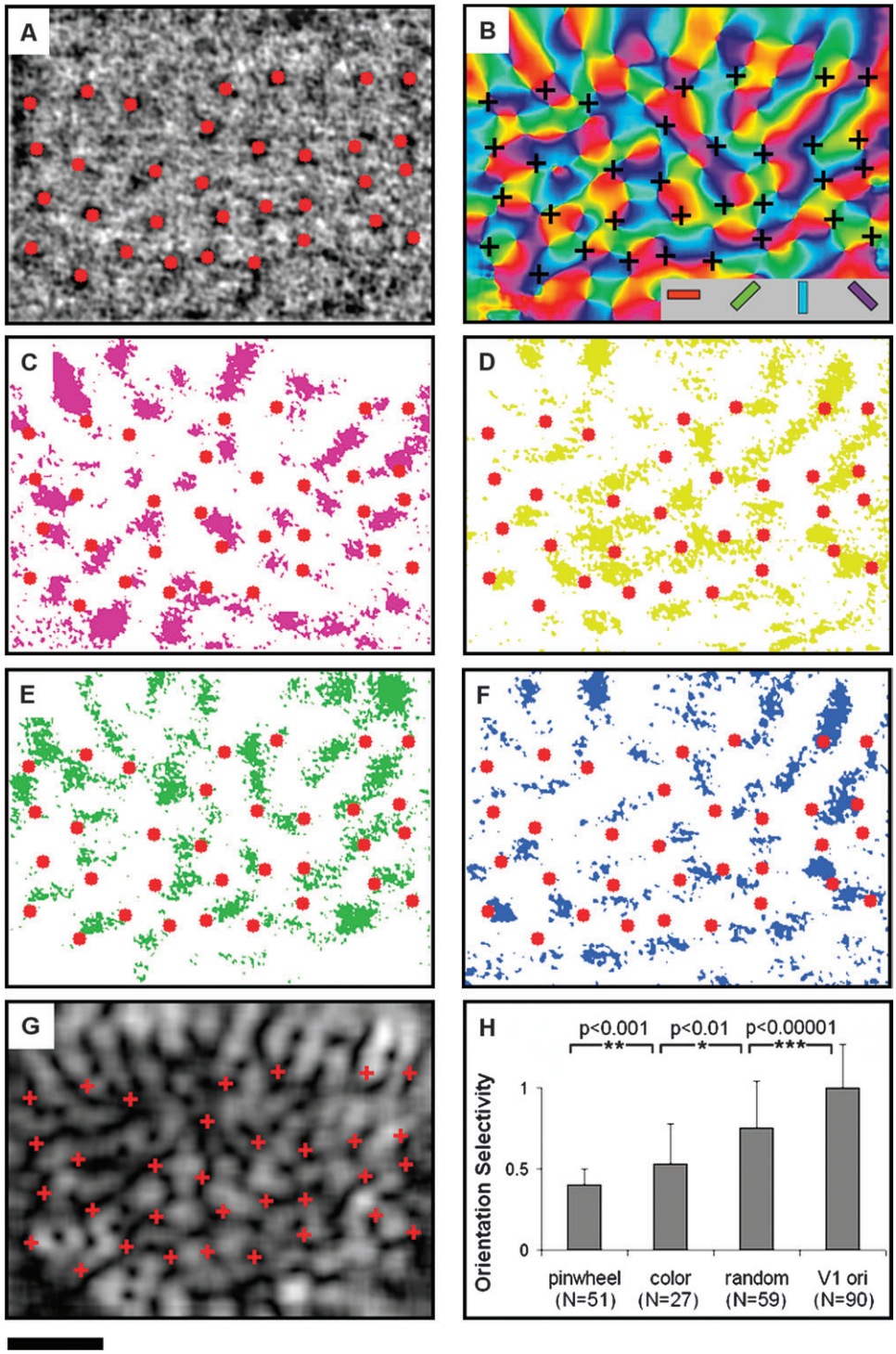

Figure 12. Blobs are regions of low orientation selectivity. Case 3 (in this case, a 1.25 c/deg thin white line grating was used for obtaining OD and orientation maps). (*A*) Color activation map, same as Figure 8*A*, blob locations marked with red dots. (*B*) orientation selectivity vector map with color code in insert. (*C*–*F*) Threshholded single-condition maps for 0°, 45°, 90°, 135° gratings, respectively. Red dots represents blob locations. (*G*) orientation selectivity magnitude map from vector analysis. Black pixels indicate low orientation selectivity. (*H*) Comparison of orientation selectivity (based on pixel values in *G*) among 4 different regions: pinwheels, blobs, orientation domains, and randomly selected locations. Bar values are averaged over all the pixels in a specific domain and normalized to the mean value in V1 orientation domain. These 4 types of domains are all different from each other (*t*-test, $*P < 0.05$, $**P < 0.001$, $***P < 0.00001$). Error bar is SD. Scale bar: 1 mm applies to figures (*A*)–(*G*).

orientation selectivity. We also find that color domains are unlikely to coincide with orientation pinwheels, as orientation selectivity of pinwheels is significantly lower than that of color domains. However, the identity and stability of orientation pinwheels remains controversial (e.g., Polimeni et al. 2005), and the low orientation selectivity at pinwheel locations maybe a result of the resolution limit of intrinsic optical imaging, instead of the real orientation selectivity of cells (see Ohki et al. 2006). Interestingly, the ratio of color domains to iso-orientation domains is comparable, supporting the original hypothesis of

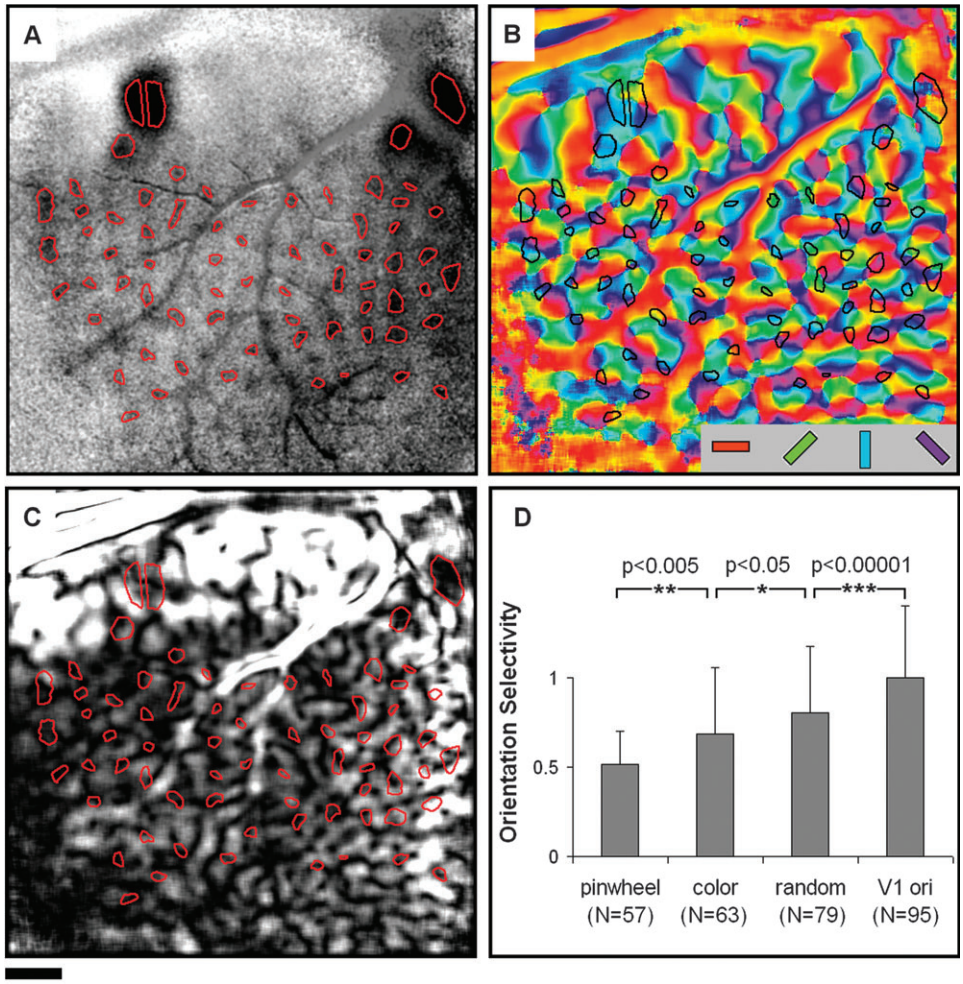

Figure 13. Blobs are regions of low orientation selectivity. Case 1. (*C*) Color maps (same as Fig. 1*D*) with color mask overlain. (*B*) Orientation selectivity vector map with color mask overlain. Color code is indicated in inset. (*C*) Color mask overlaid on orientation selectivity magnitude map from vector analysis. (*D*) Comparison of orientation selectivity (based on pixel values in *C*) among 4 different regions: pinwheels, blobs, orientation domains, and randomly selected locations. Bar values are averaged over all the pixels in a specific domain and normalized to the mean value in V1 orientation domain. Error bar is SD. Scale bar: 1 mm, applies to (*A*)–(*C*).

a color/orientation hypercolumn (Hubel and Wiesel 1977). These data thus suggest that monocularly driven population color responses in V1 are preferentially localized to CO blobs. We suggest that the term "blob" be used as both an anatomical and functional term, one that is inclusive of concept of "CO blob" and of "color domain" in V1.

In V2, we find that color domains coincide with the thin stripes and are complementary in location to orientation domains which coincide with the thick and pale stripes. Within thin stripes, color-preferring regions only occupy part of the stripes and often have a patchy appearance (~ 650 μm in diameter). A recent study has shown that different hues activate different subregions within these color domains (Xiao et al. 2003). The color domains we imaged are larger and may represent regions that respond best to red and green colors because we use red–green gratings. It is unclear how these domains relate to the irregular patchiness apparent in some CO stains of V2 thin and thick stripes (e.g., ~250 μm in diameter, Tootell and Hamilton 1989). In our experience, cytochrome patches in V2 stripes are quite variable from monkey to monkey and also between stripes within the same monkey, due either to true variability or to variability in staining. Cytochrome patches have also been shown to align poorly with 2DG uptake after color or black/white stimulation (see Tootell and Hamilton 1989; Fig. 5). Qualitatively, our data show that the strongest red–green color responses at times align with CO dense patches (e.g., Fig. 2*C*,*D*); however, there appear to be significant differences in the extent of these 2 types of patches. Factors which limited quantitative comparison include small V2 sample size (usually only 0–3 mm of V2 is exposed on the surface) and quality of CO staining (not every CO staining reveals patchness in V2, due either to quality of staining or to variability across animals and/or across stripes). In sum, in both V1 and V2, we find evidence for functional segregation, at least at the population response level, of color and form, and that this segregation bears a strong correlation with CO-staining patterns.

The Debate

There continues to be debate, based largely on electrophysiological studies, regarding whether blobs and interblobs in V1 and thin, pale, and thick stripes in V2 in the Macaque monkey differ with respect to contrast, color, and orientation content (Livingstone and Hubel 1984; Ts'o and Gilbert 1988; Lennie et al.

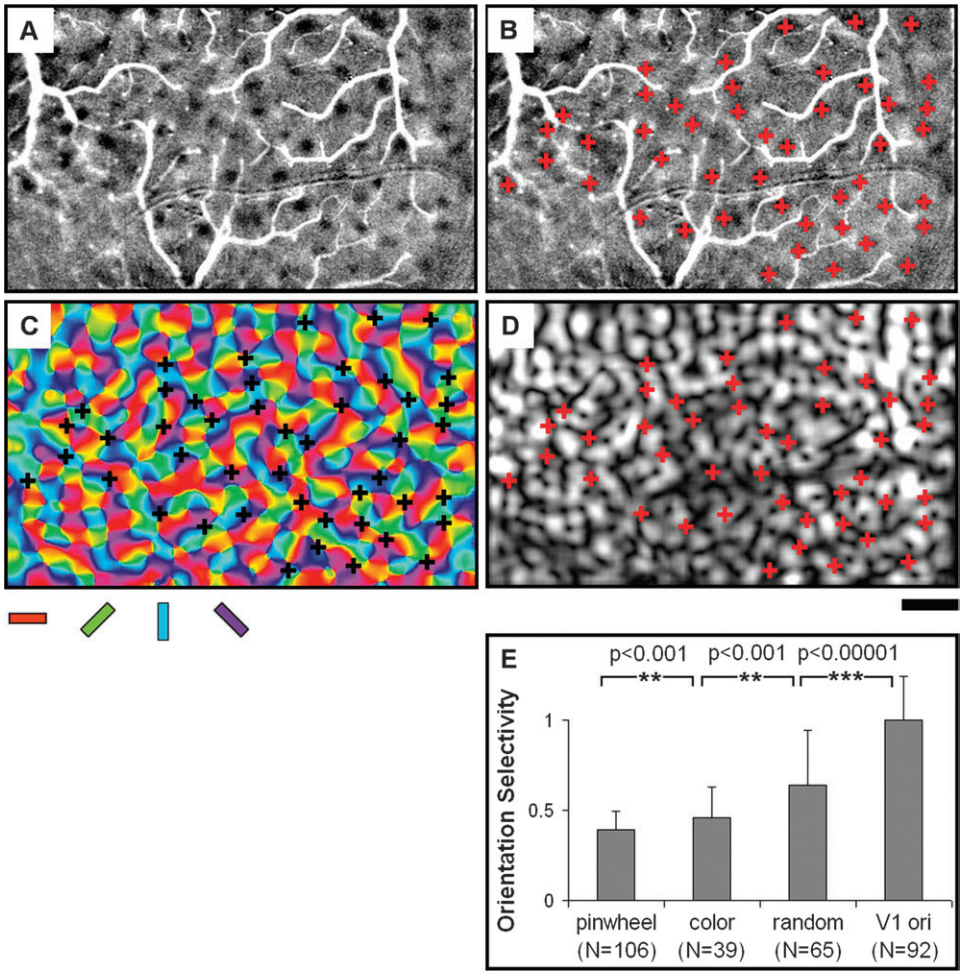

Figure 14. Blobs are regions of low orientation selectivity. Case 5. (*A*) Color activation map obtained by subtracting luminance activation from red–green isoluminant activation. (*B*) Same map as in (*A*) with blob locations marked with red crosses. (*C*) Orientation selectivity vector map with blob location marked with black crosses. Color code is indicated below. (*D*) Color markers overlaid on orientation selectivity magnitude map from vector analysis. (*E*) Comparison of orientation selectivity (based on pixel values in *C*) among 4 different regions: pinwheels, blobs, orientation domains, and randomly selected locations. Bar values are averaged over all the pixels in a specific domain and normalized to the mean value in V1 orientation domain. Error bar is SD. Scale bar: 1 mm applies to (*A*)–(*D*).

1990; Leventhal et al. 1995; Landisman and Ts'o 2002a, 2002b; Friedman et al. 2003; Sincich and Horton 2005). Currently, this controversy can be encapsulated into 2 main issues: 1) whether there is segregation in the representation of color and orientation information in V1 and 2) whether CO blobs and interblobs underlie the anatomical basis for such segregation.

The association of color selectivity and poor orientation selectivity is highly controversial. Although some studies claim an association between color selectivity and lack of orientation tuning (Livingstone and Hubel 1984; Ts'o and Gilbert 1988; Conway 2001; Landisman and Ts'o 2002b), other studies find that color-selective and orientation-selective responses are carried within single cells and that therefore color and form are not processed separately in the cortex (Lennie et al. 1990; Leventhal et al. 1995; Friedman et al. 2003). With respect to spatial distribution, electrophysiological studies have also reached different conclusions. Some have supported the view that CO blobs are centers of color preference and poor orientation preference (Livingstone and Hubel 1984; Ts'o and Gilbert 1988; Yoshioka and Dow 1996; Landisman and Ts'o 2002b; Vanduffel et al. 2002); others find no significant difference in color and orientation preference of blob and interblob domains (Lennie et al. 1990; Leventhal et al. 1995; orientation O'Keefe et al. 1998). Using orientation pinwheels as markers for orientation, Landisman and Ts'o (2002a) find a poor correspondence between pinwheels and color domains in V1. One elegantly designed electrophysiological study attempted to extrapolate population response of cytochrome blobs from single unit recordings taken at different distances from CO blob centers (Edwards et al. 1995). This study concluded that centers of blobs exhibit higher contrast gain and lower spatial frequency response, suggesting that blobs do exhibit responses functionally distinct from that of interblobs. Recent 2-photon imaging revealed a highly ordered arrangement of sharp orientation tuned cells at pinwheel centers (Ohki et al. 2006; see also Bartfeld and Grinvald 1992), further supporting the suggestion that pinwheels and CO blobs are 2 separate systems. Our results suggest a clear association of color blobs with locations of low orientation selectivity that is distinct from pinwheel locations.

Experimental factors are likely to contribute to some of these differing results. Although electrode recording sites were reconstructed in these studies, there is some intrinsic error associated with reconstruction of recording sites. Because CO

blobs are small (~200 μm in size), a small degree of error could be significant. Differences in conclusions could also be influenced by differences in sampling methods and differences in receptive field characterization (hand plots, sinusoidal isoluminant gratings, mapping with cone isolating stimuli). Clearly, electrophysiological study is the master for studying functional preferences of single cells, but may not provide consistent answers to questions of response proportion or to spatial distribution.

Questions regarding functional organization are more directly addressed by functional imaging and functional anatomical methods. Studies which reveal population responses (2-deoxyglucose [2-DG] and imaging methods) tend to support the role of blobs in the processing of low spatial frequency, color information. As shown by 2-DG methodology, blobs are preferentially activated by color-varying gratings of low and middle spatial frequencies and by spatially diffuse color stimuli (Tootell, Silverman, et al. 1988). Although these 2-DG images appeared blob-like in appearance, no alignment of the 2-DG image and CO blob pattern was performed. Optical imaging studies have shown good alignment between CO blobs and centers of monocularity (Ts'o et al. 1990) and between CO blobs and regions of poor orientation selectivity (Bartfeld and Grinvald 1992).

One study finds a more complicated correspondence between blobs and color response, one that was not a simple one-to-one relationship (Landisman and Ts'o 2002a). Of 61 color domains in the Landisman and Ts'o report, only 36% aligned with cytochrome blobs. The remainder appeared to be irregular in shape, tended to be larger than CO blobs, and were observed to span 2 or more blobs; a large fraction of these blobs (23%) crossed ocular dominance borders. However, these conclusions were based on color maps which resulted from the summing of Left eye and Right eye response maps (e.g., Fig. 6 from their paper). In our hands, when maps are noisy, variability in local vascular response can lead to weak signal which when summed with other weak signals, result in an apparent displacement of activation sites. In maps in which signals are strong, we typically observed punctate activations to red/green isoluminant stimuli, consistent with the size and spacing of CO blobs, and rarely observed activations that spanned multiple blobs or that span 2 blobs of different ocular dominance columns. This does not preclude the possibility that there may be binocular color responses in cytochrome bridges as has been demonstrated electrophysiologically by Landisman and Ts'o (2002a, 2002b). The organization of binocular color response (which could be shown by comparing binocular vs. monocular color response) has not yet been examined.

In sum, our data are consistent with work indicating the predominance of color-selective cells in blobs and supports the association of color and cytochrome blobs originally proposed by Livingstone and Hubel. We find that color-activated blobs, mapped with low spatial frequency color stimuli (isoluminant red–green gratings), are in good alignment with the CO blobs. The spacing and size of the activated domains is consistent with the cytochrome blob pattern. Furthermore, the complementary of color domains and orientation domains suggests some degree of color/contour segregation in V1. Given the number of consistent cases, the large fields of view showing good correspondence, and the multiple types of correspondence (color/blob, color/monocularity, color/low orientation selectivity), our data strongly support the view of structural and functional correlation.

Proposed Resolution

We argue that the entire body of published data, including those studies that report a lack of correspondence, can be mutually consistent. Our view is that single cortical locations contain a mixture of responses and cell types but, on average, there is organization. This organization is more easily revealed by techniques, such as the optical imaging method, which sample over large populations of neurons. It is very possible that different electrophysiological samplings can provide different views of the same cortical area. In our own experience, being able to electrophysiologically target imaged color domains increases our yield of color cells tremendously. This suggests that sampling methods can strongly influence the population response profile. Functional imaging provides, in a sense, a more "unbiased" view of the average population response. The fact that we get "blob" activation at all indicates that, on average, the cells in those locations prefer color stimuli over achromatic stimuli. Indeed, we emphasize that functional organization does not imply strict segregation, as each functional structure contains a mixture of neurons with varying selectivities. However, the fact that functional imaging and functional anatomical studies reveal blob and stripe structure suggests that there are differences in the overall population response between structures. Thus, although single neurons are multidimensional (e.g., have some degree of responsiveness to both contour orientation and to color), these findings suggest some segregation of processing with respect to contour versus color.

Supplementary Material

Supplementary material can be found at: http://www.cercor.oxfordjournals.org/.

Notes

Supported by NIH EY11744, Packard Foundation, Center for Integrative, and Cognitive Neuroscience, and P30EY008126. We thank Benjamin Ramsden for assistance in collecting data from one case. *Conflict of Interest*: None declared.

Funding to pay the Open Access publication charges for this article was provided by NEI 11744.

Address correspondence to Haidong D. Lu, Department of Psychology, Vanderbilt University, 301 Wilson Hall, 111 21st Avenue South, Nashville, TN 37203, USA. Email: haidong.lu@vanderbilt.edu.

References

Bartfeld E, Grinvald A. 1992. Relationships between orientation-preference pinwheels, cytochrome-oxidase blobs, and ocular-dominance columns in primate striate cortex. Proc Natl Acad Sci USA. 89:11905–11909.

Blasdel GG. 1992a. Differential imaging of ocular dominance and orientation selectivity in monkey striate cortex. J Neurosci. 12:3115–3138.

Blasdel GG. 1992b. Orientation selectivity, preference, and continuity in monkey striate cortex. J Neurosci. 12:3139–3161.

Bonhoeffer T, Grinvald A. 1991. Iso-orientation domains in cat visual cortex are arranged in pinwheel-like patterns. Nature. 353:429–431.

Born RT, Tootell RB. 1991. Spatial frequency tuning of single units in macaque supragranular striate cortex. Proc Natl Acad Sci USA. 88:7066–7070.

Bosking WH, Zhang Y, Schofield B, Fitzpatrick D. 1997. Orientation selectivity and the arrangement of horizontal connections in tree shrew striate cortex. J Neurosci. 17:2112–2127.

Conway BR. 2001. Spatial structure of cone inputs to color cells in alert macaque primary visual cortex (V-1). J Neurosci. 21:2768–2783.

Edwards DP, Purpura KP, Kaplan E. 1995. Contrast sensitivity and spatial frequency response of primate cortical neurons in and around the cytochrome-oxidase blobs. Vision Res. 35:1501–1523.

Friedman HS, Zhou H, von der Heydt R. 2003. The coding of uniform colour figures in monkey visual cortex. J Physiol. 548:593–613.
Gegenfurtner KR, Kiper DC, Fenstemaker SB. 1996. Processing of color, form, and motion in macaque area V2. Vis Neurosci. 13:161–172.
Horton JC. 1984. Cytochrome-oxidase patches: a new cytoarchitectonic feature of monkey visual cortex. Philos Trans R Soc Lond B Biol Sci. 304:199–253.
Horton JC, Hocking DR. 1996. Intrinsic variability of ocular dominance column periodicity in normal macaque monkeys. J Neurosci 16:7228–7239.
Horton, JC, Hubel DH. 1981. Regular patchy distribution of cytochrome oxidase staining in primary visual cortex of macaque monkey. Nature. 292:762–764.
Hubel DH, Livingstone MS. 1987. Segregation of form, color, and stereopsis in primate area 18. J Neurosci. 7:3378–3415.
Hubel DH, Wiesel TN. 1977. Ferrier lecture. Functional architecture of macaque monkey visual cortex. Proc R Soc Lond B Biol Sci. 198:1–59.
Landisman CE, Ts'o DY. 2002a. Color processing in macaque striate cortex: relationships to ocular dominance, cytochrome oxidase, and orientation. J Neurophysiol. 87:3126–3137.
Landisman CE, Ts'o DY. 2002b. Color processing in macaque striate cortex: electrophysiological properties. J Neurophysiol. 87:3138–3151.
Lennie P, Krauskopf J, Sclar G. 1990. Chromatic mechanisms in striate cortex of macaque. J Neurosci. 10:649–669.
Leventhal AG, Thompson KG, Liu D, Zhou Y, Ault SJ. 1995. Concomitant sensitivity to orientation, direction, and color of cells in layers 2, 3, and 4 of monkey striate cortex. J Neurosci. 15:1808–1818.
Levitt JB, Kiper DC, Movshon JA. 1994. Receptive fields and functional architecture of macaque V2. J Neurophysiol. 71:2517–2542.
Livingstone MS, Hubel DH. 1984. Anatomy and physiology of a color system in the primate visual cortex. J Neurosci. 4:309–356.
Lu HD, Roe AW. 2007. Optical imaging of contrast response in macaque monkey V1 & V2. Cereb Cortex. doi:10.1093/cercor/bhl177.
Malach R, Tootell RB, Malonek D. 1994. Relationship between orientation domains, cytochrome-oxidase stripes, and intrinsic horizontal connections in squirrel monkey area V2. Cereb Cortex. 4:151–165.
Maldonado PE, Godecke I, Gray CM, Bonhoeffer T. 1997. Orientation selectivity in pinwheel centers in cat striate cortex. Science. 276:1551–1555.
Murphy KM, Jones DG, Fenstemaker SB, Pegado VD, Kiorpes L, Movshon JA. 1998. Spacing of cytochrome oxidase blobs in visual cortex of normal and strabismic monkeys. Cereb Cortex. 8:237–244.
O'Keefe LP, Levitt JB, Kiper DC, Shapley RM, Movshon JA. 1998. Functional organization of owl monkey lateral geniculate nucleus and visual cortex. J Neurophysiol. 80:594–609.
Ohki K, Chung S, Kara P, Hbener M, Bonhoeffer T, Reid RC. 2006. Highly ordered arrangement of single neurons in orientation pinwheels. Nature. 442:925–928.
Peterhans E, von der Heydt R. 1993. Functional organization of area V2 in the alert macaque. Eur J Neurosci. 5:509–524.
Polimeni JR, Granquist-Fraser D, Wood RJ, Schwartz EL. 2005. Physical limits to spatial resolution of optical recording: clarifying the spatial structure of cortical hypercolumns. Proc Natl Acad Sci USA. 102:4158–4163.
Ramsden BM, Hung CP, Roe AW. 2001. Real and illusory contour processing in area V1 of the primate: a cortical balancing act. Cereb Cortex. 11:648–665.
Roe AW. 2003. Modular complexity of Area V2 in the macaque monkey. In: Kaas J, Collins C, editors. The primate visual system. New York (NY): CRC Press. p. 109–138.
Roe AW, Lu HD. 2006. Functional organization of color domains in V1 and V2 of Macaque monkey revealed by optical imaging [VSS 2006 Abstract]. J Vis. 6:405a.
Roe AW, Ts'o DY. 1995. Visual topography in primate V2: multiple representation across functional stripes. J Neurosci. 15: 3689–3715.
Roe AW, Ts'o DY. 1999. Specificity of color connectivity between primate V1 and V2. J Neurophysiol. 82:2719–2730.
Schummers J, Marino J, Sur M. 2002. Synaptic integration by V1 neurons depends on location within the orientation map. Neuron. 36:969–978.
Shoham D, Hubener M, Schulze S, Grinvald A, Bonhoeffer T. 1997. Spatio-temporal frequency domains and their relation to cytochrome-oxidase staining in cat visual cortex. Nature. 385:529–533.
Silverman MS, Grosof DH, De Valois RL, Elfar SD. 1989 Spatial-frequency organization in primate striate cortex. Proc Natl Acad Sci USA. 86:711–715.
Sincich LC, Horton JC. 2005. Input to V2 thin stripes arises from V1 cytochrome-oxidase patches. J Neurosci. 25:10087–10093.
Tootell RB, Hamilton SL. 1989. Functional anatomy of the second visual area (V2) in the macaque. J Neurosci. 9:2620–2644.
Tootell RB, Hamilton SL, Silverman MS, Switkes E. 1988a. Functional anatomy of macaque striate cortex. I. Ocular dominance, binocular interactions, and baseline conditions. J Neurosci. 8:1500–1530.
Tootell RB, Silverman MS, Hamilton SL, De Valois RL, Switkes E. 1988c. Functional anatomy of macaque striate cortex. III. Color. J Neurosci. 8:1569–1593.
Tootell RB, Switkes E, Silverman MS, Hamilton SL. 1988b. Functional anatomy of macaque striate cortex. II. Retinotopic organization. J Neurosci. 8:1531–1568.
Ts'o DY, Frostig RD, Lieke EE, Grinvald A. 1990. Functional organization of primate visual cortex revealed by high resolution optical imaging. Science. 249:417–420.
Ts'o DY, Gilbert CD. 1988. The organization of chromatic and spatial interactions in the primate striate cortex. J Neurosci. 8:1712–1727.
Ts'o DY, Roe AW, Gilbert CD. 2001. A hierarchy of the functional organization for color, form and disparity in primate visual area V2. Vision Res. 41:1333–1349.
Vanduffel W, Tootell RB, Schoups AA, Orban GA. 2002. The organization of orientation selectivity throughout Macaque visual cortex. Cereb Cortex. 12:647–662.
Vnek N, Ramsden BM, Hung CP, Goldman-Rakic PS, Roe AW. 1999. Optical imaging of functional domains in the cortex of the awake and behaving monkey. Proc Natl Acad Sci USA. 96:4057–4060.
Wang Y, Xiao Y, Felleman DJ. 2007. V2 thin stripes contain spatially organized representations of achromatic luminance change. Cereb Cortex. 17:116–129.
Wong-Riley M. 1979. Related Changes in the visual system of monocularly sutured or enucleated cats demonstrable with cytochrome-oxidase histochemistry. Brain Res. 171:11–28.
Xiao Y, Wang Y, Felleman DJ. 2003. A spatially organized representation of colour in macaque cortical area V2. Nature. 421:535–539.
Xu X, Bosking W, Sary G, Stefansic J, Shima D, Casagrande V. 2004. Functional organization of visual cortex in the owl monkey. J Neurosci. 24:6237–6247.
Yoshioka T, Dow BM. 1996. Color, orientation and cytochrome-oxidase reactivity in areas V1, V2 and V4 of macaque monkey visual cortex. Behav Brain Res. 76:71–88.